



Universiteit
Leiden
The Netherlands

Protein film electrochemistry

Butt, J.N.; Jeuken, L.J.C.; Zhang, H.; Burton, J.A.J.; Sutton-Cook, A.L.

Citation

Butt, J. N., Jeuken, L. J. C., Zhang, H., Burton, J. A. J., & Sutton-Cook, A. L. (2023). Protein film electrochemistry. *Nature Reviews Methods Primers*, 3(1).
doi:10.1038/s43586-023-00262-7

Version: Accepted Manuscript

License: [Licensed under Article 25fa Copyright Act/Law \(Amendment Taverne\)](#)

Downloaded from: <https://hdl.handle.net/1887/3753412>

Note: To cite this publication please use the final published version (if applicable).

Protein film electrochemistry

Julea N. Butt^{1†}, Lars J. C. Jeuken^{2†}, Huijie Zhang², Joshua A. J. Burton¹, Alexander L. Sutton-Cook¹

¹School of Chemistry and School of Biological Sciences, University of East Anglia, Norwich Research Park, Norwich, NR4 7TJ, U.K.

²Leiden Institute of Chemistry, Leiden University, PO box 9502, Leiden 2300 RA, The Netherlands

†e-mail: j.butt@uea.ac.uk, l.j.c.jeuken@lic.leidenuniv.nl

ABSTRACT: Protein Film Electrochemistry (PFE) is a powerful suite of electroanalytical techniques used to investigate the properties of redox proteins. The proteins under investigation are adsorbed as a (sub-)monolayer film on an electrode surface. Direct electron transfer between the immobilized protein and working electrode gives rise to an electrical current that visualizes and quantifies redox processes occurring within the protein. Advantages of PFE include low sample requirements — typically less than a nanomole protein — high sensitivity and the ability to resolve redox chemistry in the electrochemical potential and time domains. This Primer provides a guide to using PFE for quantitative thermodynamic and kinetic descriptions of half-reactions (redox reactions) and coupled chemical processes, including ligand binding, ligand unbinding and redox catalysis. Applications of PFE in developing biosensors, facilitating energy conversion and resolving enzyme mechanisms are highlighted. Finally, the state-of-the-art and prospects for novel experimental and theoretical approaches are discussed.

INTRODUCTION

Redox proteins are ubiquitous in biology. They perform electron transfer reactions and redox catalysis that are essential to life, for example, in photosynthesis and respiration. These functions are enabled by redox active cofactors, one or more per protein, including copper, molybdenum, heme, non-heme iron and flavin^{1,2}. During physiologically relevant electron exchange the redox cofactors are positioned within 14 Å of one another³. Electron transfer between proteins is supported by cofactors near the protein surface. By contrast, redox catalysis may occur adjacent to cofactors buried deep within a peptide matrix. This allows redox transformation of the substrate in a site shielded from solvent, avoiding non-productive and possibly toxic redox reactions. Additional redox cofactors positioned as a chain enable electrons to be relayed between the active site and protein surface, **FIG. 1A**.

Protein film electrochemistry (PFE) — also termed protein film voltammetry (PFV) and protein monolayer electrochemistry — is a powerful tool for investigating the properties of redox proteins⁴⁻¹¹. PFE studies protein electron transfer and redox catalysis using dynamic electrochemistry applied to a (sub-)monolayer film of redox active protein immobilised on the surface of a working electrode (WE). As shown schematically in **FIG. 1A**, there is direct electron exchange between the immobilised protein and WE, which gives rise to an electric current. The produced current visualises and quantifies redox processes within the protein. Using this approach, quantitative thermodynamic and kinetic descriptions of half-reactions (redox reactions) and coupled chemical processes, including redox catalysis, can be readily obtained. These descriptions result from considering direct electron transfer between the WE and adsorbed protein, **FIG. 1A**. PFE is different to experiments that use mediated electron transfer, where an additional redox-active species, often called a mediator, is introduced to shuttle electrons between the protein and WE.

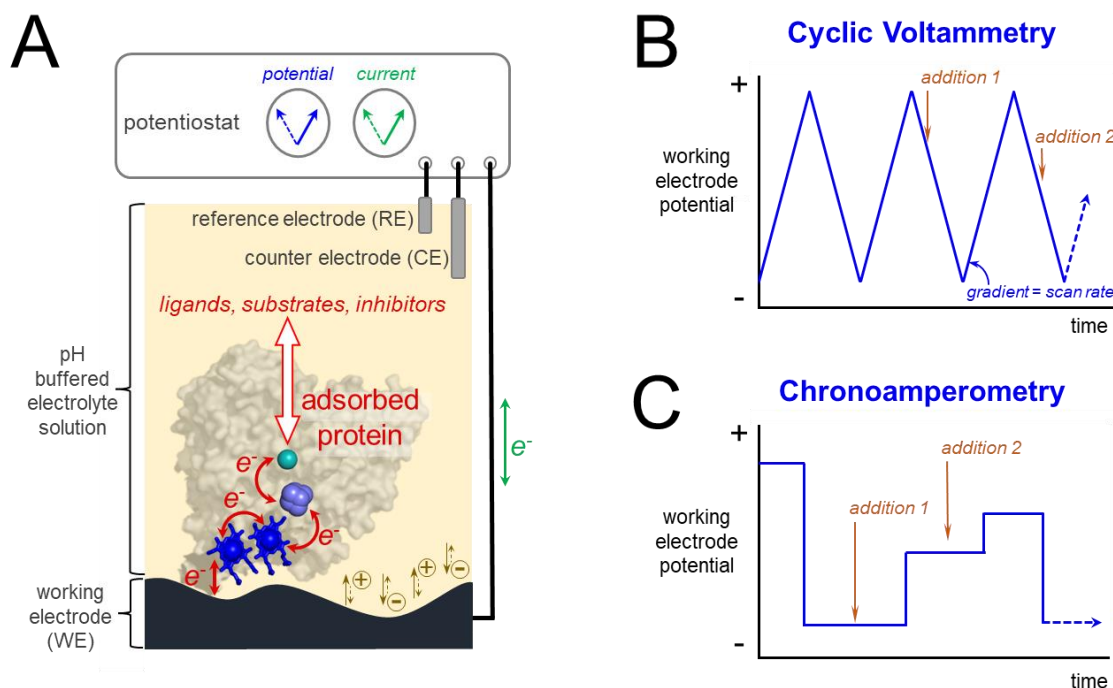


Fig. 1 | Concept of protein film electrochemistry (PFE). **A** | The protein of interest is adsorbed as a (sub-)monolayer film on a working electrode (WE). Direct electron transfer occurs between the WE and a redox cofactor terminating a chain of additional redox sites within the protein: heme (royal blue), iron-sulphur cluster (navy) and Mo (teal) cofactors (PDB ID: 1OGY). The protein retains full activity towards molecules and/or ions introduced to the surrounding electrolyte solution. The Mo cofactor is the active site of this redox enzyme. The hemes and iron-sulphur cluster relay electrons between the active site and the WE. A potentiostat applies defined and variable potential to the WE while simultaneously measuring the flow of current through that electrode. The measured current has two contributions: Faradaic current due to redox transformation in the protein (red arrows), capacitance due to migration of electrolyte ions (brown arrows). **B** | The excitation profile applied during cyclic voltammetry (CV) illustrating how scan rate is defined. **C** | An excitation profile for chronoamperometry (CA). Brown arrows indicate that reactants can be introduced at desired times in both CV (B) and CA (C).

43 PFE traces its roots back to the 1990s, when electrochemistry of adsorbed proteins was reported^{12, 13}
 44 ¹⁴ that agreed with the properties defined by established biochemical assays of proteins in solution⁶.
 45 The adsorbed proteins retained functional integrity and the electrode-protein interactions could be
 46 considered to mimic those between the protein of interest and its biological redox partner. Today the
 47 advantages of PFE for revealing and understanding redox protein activity are widely recognised. The
 48 equipment is extremely low cost compared to modern biophysical methods and spectroscopies, with
 49 lower protein requirements, often sub-picomole in an adsorbed film prepared from a solution of less
 50 than a nanomole protein. The protein-coated electrode often survives changes in the solution to
 51 which it is immersed, meaning the impact of varying conditions can be readily assessed. Signals are
 52 sharp and high-resolution, enabling complex behaviour to be controlled, dissected, and elucidated
 53 because there are no contributions from relatively slow protein diffusion. In a single experiment, the
 54 current is measured across a wide, continuous potential range for the desired time — from under a
 55 second to several hours — allowing many different and defined changes to be made to the
 56 composition, pH and temperature of the immersion solution.

57 This Primer will describe the equipment typically used for PFE and provide the practical and theoretical
 58 background needed to perform and interpret electrochemical experiments. The article focuses on
 59 explaining how standard concepts available in electrochemistry^{15,16} and biochemistry¹⁷ textbooks

60 typically apply to PFE, illustrating how PFE describes redox couples, ligand binding and redox catalysis.
61 Detailed discussions are kept to the simplest scenarios. However, more complex behaviours are
62 touched upon, with references to works that illustrate how those results may be investigated and
63 explained.

64 In this Primer, cyclic voltammetry (CV) and chronoamperometry (CA) will be focused on, as they are
65 widely used and provide the most immediately intuitive and quantitative descriptions of protein redox
66 chemistry. In CV, the WE potential is swept back and forth across a region of interest at a specified
67 scan rate, **FIG. 1B**. The resulting current is measured simultaneously and reported as a cyclic
68 voltammogram that plots current versus WE potential. In CA, the potential of the WE is stepped
69 instantaneously between defined values at specified time points, **FIG. 1C**. The resulting current is
70 reported versus time in an amperograms. Conditions can be changed as desired, for instance, a
71 reactant can be introduced in both types of experiment.

72 It is important to recognise that the current in both CV and CA has two components that are
73 superimposed¹⁵. The Faradaic current is due to electron transfer between the electrode and redox
74 active proteins in the (sub-)monolayer film, **FIG. 1A** (red arrows). Non-Faradaic current (capacitance)
75 is due to charging and discharging of the electrode–solution interface and electrons are not
76 transferred across that interface, **FIG. 1A** (brown arrows). PFE is interested in the Faradaic current, as
77 it reports the redox chemistry of the protein. Care must be taken to accurately extract the Faradaic
78 current from the measured current. By convention, Faradaic current is negative during net reduction
79 and positive for net oxidation.

80

81 **EXPERIMENTATION**

82 The equipment needed for PFE depends on the desired application, but requires at least a
83 potentiostat¹⁸, an electrochemical cell and analytical software. The electrochemical cell contains a
84 counter electrode (CE) and reference electrode (RE) in addition to the WE. During measurements the
85 WE may be stationary or rotating. The latter is particularly useful when studying redox catalysis and a
86 rotating disk electrode (RDE)¹⁵ allows controlled substrate delivery to the adsorbed enzyme. These
87 experiments can be extended to use a rotating ring disk electrode (RRDE)¹⁵, which forces the products
88 of enzyme catalysis to flow across a second WE — a concentric ring around the central enzyme coated
89 disk electrode — for analysis by amperometry.

90 ***Potentiostats and working electrode rotators***

91 Potentiostats can be purchased from many manufacturers. Alternatively, the instrument can be made
92 in-house¹⁹ for a fraction of the cost. The ideal instrument will depend on the specific requirements
93 and funds available. All potentiostats can perform basic CV and CA methods. The specifications that
94 require special attention for PFE are current range; scan rate or band width range; capacity for iR
95 compensation, where I is current and R is resistance; ability to use RRDEs; and ability to perform
96 analogue CV by applying a true linear voltage ramp to the WE, **FIG. 1B**, in addition to CV, which
97 approximates the linear ramp with a staircase waveform, and is the primary CV method in
98 contemporary potentiostats¹⁸.

99 PFE typically uses WEs with a surface area of $< 1 \text{ cm}^2$, scan rates in CV $< 100 \text{ V/s}$ and potential steps in
100 CA of $< 1 \text{ V}$. Under these conditions, currents are in the nA to mA range, which is adequately covered
101 by all commercial potentiostats. However, if the intended applications are in bioelectrocatalysis with
102 WEs that have larger surface areas, higher current ranges might be required.

103 When studying the kinetics of electron transfer or coupled reactions, fast-scan CV (scan rate >100
104 mV/s) is a powerful tool^{6,20-22}. As a result, the scan rate capabilities of the potentiostat should be
105 considered. The area under a redox peak, the non-catalytic CV, can deviate from theory when using
106 staircase CV²³, which is the standard method in most contemporary potentiostats¹⁸. If the protein
107 coverage analysis needs to be accurate or when studying reaction kinetics, potentiostats that can
108 measure analog CV should be considered.

109 For both non-catalytic fast scan and catalytic PFE, currents in the high μA to mA range can be obtained.
110 This can lead to significant potential drops due to solution resistance²⁴. As current flows through the
111 electrochemical cell, a potential difference is required across the electrolyte solution to drive ion
112 mobility and overcome solution resistance. As a result, the potential at the WE interface has a lower
113 magnitude than the potential applied by the potentiostat. For instance, if the solution resistance is
114 $100\ \Omega$, a current of $100\ \mu\text{A}$ leads to a potential shift of $10\ \text{mV}$ ($V = iR$, where V is potential). Potential
115 drop can be reduced by minimizing the solution resistance, but can also be compensated for by
116 potentiostats with iR compensation capabilities²⁴.

117 The sensitivity of potentiostats to electronic noise¹⁸ is an important property. However, this property
118 cannot be determined from specifications and can only be established by trying different potentiostats
119 under laboratory conditions. Where possible, the electrochemical cell should be placed in a Faraday
120 cage to reduce electronic noise. Suitable Faraday cages are readily constructed from commercially
121 sourced electrical boxes, typically steel, with holes for the electrical leads. Alternatively, Faraday cages
122 can be made from a wire mesh, which enables the electrochemical cell to be observed during
123 measurements, plus easy access for electrical leads and other connections, such as gas lines.

124 Rotators for use with RDEs are available from several suppliers. Differences include the ability to use
125 RRDEs, an integrated enclosure for the rotator shaft, variable distances between the controller and
126 rotator shaft, and the range of electrodes and electrochemical cells compatible with the rotator. The
127 choice of instrument will be influenced by the ring and disk electrode materials, and whether the
128 electrochemical cell needs to be serviced by gas supply lines or temperature-controlled water.
129 Anaerobic experiments also need to consider how readily the rotator can be positioned and operated
130 within a nitrogen-filled chamber.

131 ***Electrochemical cells, CE and RE***

132 There are many manufacturers of electrochemical cells, cEs and rEs. For many PFE applications, a
133 tailor-made electrochemical cell is worth considering, but requires access to a glass blower or fine-
134 mechanical facility. The wide range of PFE applications means there is no single best cell design.
135 Variables to consider include the distance between the RE and WE, the need for a RDE or RRDE, and
136 auxiliary methods, such as illumination for photo-electrochemistry^{25,26} or combination with
137 microscopy or spectroscopy²⁷. In **FIG. 2**, several example cell designs are provided with a short
138 explanation of their properties and specific applications.

139 Alongside the cell, the three electrodes — or four electrodes for a RRDE — are key to PFE. The CE
140 ensures electroneutrality of the electrolyte solution. For every Faradaic electron transfer at the WE,
141 an opposite electron transfer is required at the CE. In PFE, the CE is almost always platinum.
142 Electrochemical currents in PFE are typically low mA or less, meaning a small platinum wire (< 2 cm)
143 is sufficient. The most used and convenient RE is Ag/AgCl (saturated KCl) although others can be used.
144 Trace amounts of chloride ions, which leak out of the RE into the electrolyte, can affect the results for
145 some applications. In this case, a double junction RE is advised, where the Ag/AgCl RE is placed inside
146 a jacket. This can be achieved by sourcing a double-junction RE or by designing an electrochemical cell

147 with a double junction, **FIG. 2B,C**. Drift from the quoted potential¹⁵ can occur if the RE is not
 148 maintained. rEs are easily calibrated by comparing the open cell potential with respect to a trusted
 149 RE. If a trusted RE is not available, the CV of a redox couple with known reduction potential — such as
 150 ferri/ferrocyanide — can be measured under controlled temperature, pH and ionic strength.
 151 Potentials measured versus a Ag/AgCl (saturated KCl) RE at 25°C are typically converted to values
 152 versus the standard hydrogen electrode (SHE) by adding +0.197 V¹⁵.

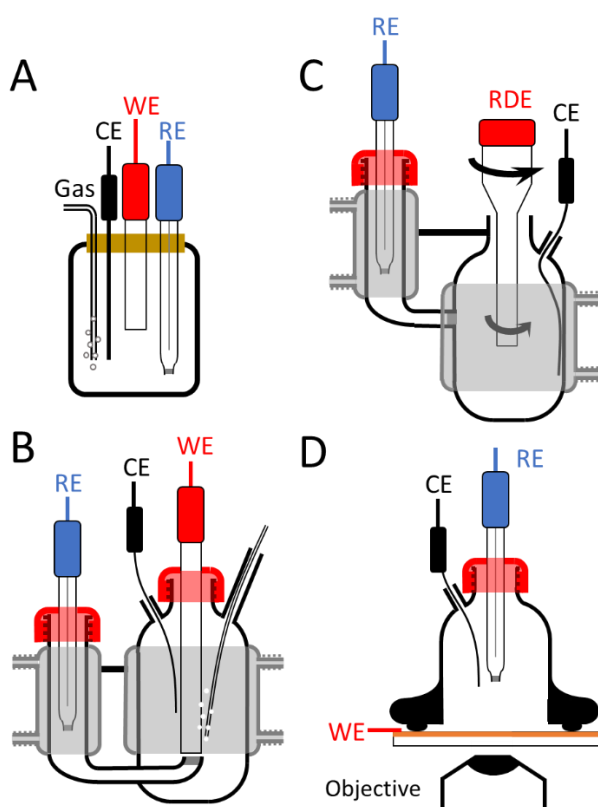


Fig. 2 | **Schematics of electrochemical cells.** (WE = working electrode; CE = counter electrode; RE = reference electrode). **A** | A basic electrochemical cell such as can be purchased commercially for use with a rod-shaped WE. **B** | An optimised electrochemical cell for stationary electrochemistry with a rod-shaped WE. The main cell has a water jacket (grey) for temperature control. The RE is placed to the side of the main cell to enable separate temperature control. Leakage of RE solution (for instance saturated KCl solution) into the main cell is minimised by using a second junction (either a glass frit or a luggin capillary). The second junction is placed close to the WE to minimize solution resistance (R) and hence potential drop (iR drop). **C** | Cell for use with a rotating disk electrode (RDE). The WE is a disk on the lower face of the rotated housing. The cell volume should be sufficiently large to preclude a significant drop of substrate concentration during measurement of redox catalysis. The CE and luggin tip are positioned to minimise turbulence. **D** | A basic electrochemical cell for working with a plate-shaped WE. If a transparent gold electrode is used — for example a <50 nm thick gold film on a glass slide — this cell can be combined with epifluorescent microscopy in an inverted microscope. Here, the glass cell is placed on top of the WE with an O-ring, which is not air-tight, and oxygen can slowly diffuse to the plate electrode from the side.

153

154 **Working electrodes**

155 In PFE, the most important electrode is the WE. To form an electroactive protein film, the redox
 156 protein needs to be immobilised on the WE while retaining its native tertiary and quaternary structure
 157 and activity. Proteins can be physisorbed or chemisorbed on the electrode surface, with physisorption
 158 being the most common²⁸. Many proteins are adsorbed via electrostatic interactions, although rarer
 159 hydrophobic interactions are known. Electrostatic interaction and protein immobilisation are affected
 160 by the ionic strength and pH of the electrolyte, as the pH determines the charge on the protein surface.
 161 Electrolyte solutions in PFE are always pH buffered. To control the potential drop across the WE
 162 without disrupting the electrostatic interaction between the protein and WE, an ionic strength of ~0.1
 163 M is often a good compromise. Adsorption/desorption is an entropic process, making temperature an

164 important variable. Lower temperatures improve the film stability but lower catalytic rates.
165 Chemisorption can be achieved by reacting an amino acid side chain group with the electrode surface²⁹
166 or by affinity interaction³⁰. Chemisorbing proteins is more time-consuming than physisorption but can
167 lead to more stable protein films³¹.

168 Electron transfer rates decrease exponentially with distance between the donor and acceptor.
169 Suitable electron transfer kinetics (< ms) for PFE requires the distance between at least one redox
170 cofactor and the electrode surface to be less than 2 nm. In practice this means that the protein needs
171 to orient correctly upon adsorption, **FIG. 1A**. One approach is to use a heterogeneous electrode
172 surface, in terms of both geometric structure and surface chemistry. Heterogeneity increases the
173 possibility that some immobilised proteins are correctly orientated, even if most are electrochemically
174 silent.

175 Three widely used WE materials are pyrolytic graphite edge (PGE) plane, modified gold and indium-
176 tin oxide (ITO), although others have successfully been used. The surface of PGE electrodes exposes
177 the side edges of the graphene sheets, enabling the carbon interface to form a rough surface with
178 multiple carbon oxide chemistries. PGE electrodes are quickly and easily cleaned by polishing the
179 surface with an aqueous slurry of alumina or diamond powder, typically 1-micron particles, followed
180 by a brief treatment in a water-bath sonicator to remove particles. This quick preparation means PGE
181 electrodes are a convenient experimental tool. The PGE surface is negatively charged due to presence
182 of carboxylic acids. Consequently, co-adsorbates are required for redox proteins that are negatively
183 charged or have a negative surface charge close the co-factor orientated towards the electrode
184 surface. Good co-adsorbates are polylysine, neomycin or polymyxin B, which are added to the
185 electrolyte or protein solution before they are applied to the electrode. The surface of PGE and other
186 graphite electrodes can also be controlled by adsorption of polycyclic aromatic hydrocarbon
187 derivatives, such as pyrene derivatives, which form stable pi-stacking interactions³². Alternatively, PGE
188 can be chemically modified to alter its surface chemistry by electrografting. For instance, reduction of
189 aryl diazonium salts forms radical anions that covalently bind with the carbon surface³³.

190 Barring some exceptions, bare gold is not a suitable electrode for PFE. However, gold electrodes have
191 surface chemistry that can be controlled by forming self-assembled monolayers (SAMs) of thiol-
192 derivatives, where the thiols form a stable gold-thiol bond³⁴⁻³⁷. This enables careful optimisation of
193 the electrode surface chemistry by forming reproducible hydrophilic/hydrophobic surfaces with
194 negative and/or positive groups. Gold electrodes can be crystalline, ultrasmooth, rough or prepared
195 from nanoparticles. The exact geometry of the gold electrode affects the structure of the SAM³⁴, which
196 affects the protein film formation and PFE results. PFE is typically performed with freshly prepared
197 SAMs. A drawback of using modified gold electrodes is that SAMs are typically formed over many
198 hours, limiting the number of experiments that can be performed in a day.

199 ITO electrodes are increasingly being used. They are optically transparent, enabling simultaneous
200 absorbance spectroscopy or photobioelectrochemistry. To increase the electrode area and roughness,
201 ITO nanoparticles can be used to create mesoporous surfaces with greater opportunity for protein
202 adsorption³⁸⁻⁴⁰. Preparation methods include using polystyrene beads as a template, around which the
203 ITO nanoparticles are deposited. This results in more highly ordered^{38,41}, honeycomb-like electrode
204 materials than direct electrophoretic deposition⁴⁰.

205 **Film preparation**

206 The protein film is typically prepared by briefly incubating the freshly polished or prepared WE surface
207 in a small volume of protein solution, just enough to wet the surface, typically μM concentration.

208 Longer incubation times may be used with more dilute protein solutions. Loosely bound material may
209 be removed from the WE surface by rinsing with an appropriate pH buffered-electrolyte solution
210 before the electrode is introduced to the electrochemical cell. It is advised that the film forming
211 solution not be allowed to dry on the WE. If the solution does dry on the WE, it can result in behaviour
212 that is difficult to reconcile with established biochemical assays, presumably due to partial or complete
213 loss of protein structure on adsorption.

214 ***Anaerobicity and temperature***

215 For experiments with applied WE potentials of approximately -0.1 V vs SHE and lower, oxygen needs
216 to be removed from the electrolyte, unless the aim is to measure oxygen interaction with the protein
217 film. For stationary electrodes, purging the electrolyte with nitrogen or argon gas is typically sufficient.
218 For lengthy experiments (> hours), gas that has been humidified by bubbling through water can be
219 used to reduce solution evaporation, which would change the ionic strength or pH of the electrolyte.
220 When using a RDE, anaerobicity can be achieved with closed electrochemical cells, as the rotating
221 electrode stirs the electrolyte, rapidly drawing in air or gas. Closed RDE systems can be challenging to
222 design. Open systems may be preferred and are most readily used within a glove box — a N₂-filled
223 chamber — to ensure anaerobic conditions.

224 Temperature is an important parameter because it is a primary determinant of reaction rate.
225 Temperature is most conveniently controlled by placing the electrochemical cell in a temperature-
226 controlled solution. Commercial or tailor-made electrochemical cells can be designed with an external
227 water jacket, where the temperature is set with a circulating water bath. However, the potential of
228 the RE is temperature dependent. For accurate control of the applied potential, the RE can be placed
229 in a side-arm of the cell with its own temperature-controlled water jacket, **FIG. 2B,C**.

230 ***Software***

231 All commercial potentiostats come with software to control the hardware. This software is often able
232 to perform a basic analysis of voltammograms and amperomograms, but capabilities are very limited.
233 A versatile, freely available software is QSoas⁴²⁻⁴⁴. QSoas enables basic data analysis, such as
234 smoothing and baseline subtraction capabilities to remove non-Faradaic currents. QSoas also allows
235 non-linear curve fitting, creating a flexible fitting platform to analyse catalytic waves with complex
236 kinetic models. QSoas is still being expanded, with recent additions including calculation of redox
237 peaks at increasing scan rate.

238 Electronic noise can often be eliminated by careful design and maintenance of the electrochemical
239 equipment and its location¹⁸. If noise persists, its contribution to the measured data can be lowered
240 in several ways¹⁸. Random noise can be removed by signal averaging applied to consecutive steady-
241 state measurements. Regular, periodic noise can be removed by fast Fourier transform techniques,
242 which are included in the controlling software or QSoas. If such methods are used, it is important to
243 inspect the data carefully to ensure that key information hasn't been distorted.

244 ***Further considerations***

245 The experimental and equipment requirements outlined above are for basic PFE experiments.
246 However, there are many insightful and exciting examples where PFE is expanded beyond the basic
247 setup. These may require adjustments to the electrochemical cell and electrodes or additional
248 equipment. Examples include the use of microelectrodes^{45,46}, combining PFE with spectroscopy^{27,47-52},
249 using high or low (< 0 °C) temperatures⁵³ or specialised gas mixtures. A full discussion is beyond the
250 scope of this Primer, but three options could be considered when purchasing a potentiostat. All

251 potentiostats perform basic CV and CA, but more advanced methods, such as electrochemical
 252 impedance spectroscopy, are not standard. Impedance spectroscopy can be useful when studying
 253 SAM formation on gold WEs. When studying catalysis, a RRDE can be useful⁵⁴, but requires a
 254 potentiostat with the ability to measure two or double WEs. Finally, when using microelectrodes, the
 255 ability to accurately measure pA and sometimes fA currents is necessary.

256

257 RESULTS

258 A few scenarios can provide the basis to describe many redox-active proteins.. This section details the
 259 corresponding Faradaic currents and the information that can be extracted. Because the
 260 experimentally measured currents include both Faradaic and non-Faradaic contributions, it is
 261 important to reiterate that the latter must be subtracted from the measured currents prior to analysis,
 262 **FIG. 3A,B**. This subtraction may make use of baseline currents measured in an identical experiment
 263 without adsorbed protein⁵⁵. Alternatively, the non-Faradaic currents may be modelled using QSoas⁴²⁻
 264 ⁴⁴. Good practice is to always measure the baseline response. This measurement enables informed
 265 modelling of the charging currents and minimises the likelihood that Faradaic currents from
 266 contaminants or additives reacting directly at the electrode will be mistaken as from the protein of
 267 interest^{8,55-57}.

268 *Mapping out half-reactions*

269 Reversible oxidation and reduction of an adsorbed protein by varying the WE potential can be
 270 described by a half-reaction: Ox + ne⁻ → Red. When this process is uncomplicated by slow interfacial
 271 electron transfer kinetics or coupling with a chemical reaction, cyclic voltammetry reveals peaks that
 272 are superposed on the non-Faradaic baseline response. These peaks are mirror images along the
 273 potential axis, **FIG. 3A,B**. Peaks detected when sweeping to increasingly positive WE potentials
 274 correspond to protein oxidation and have positive currents. Peaks with negative currents that are
 275 measured by sweeping to increasingly negative WE potentials describe cofactor reduction. Such peaks
 276 are sometimes termed non-catalytic because they do not arise from redox catalysis. When
 277 interpreting each non-catalytic peak, the current magnitude, $|i|$, can be described by^{15,58}:

278 Equation (1)

$$279 \quad |i| = \frac{\exp\left(\frac{nF}{RT}(E - E^0)\right)}{\left(1 + \exp\left(\frac{nF}{RT}(E - E^0)\right)\right)^2} \cdot \frac{n^2 F^2 v A \Gamma}{RT}$$

280 where E is the WE potential, E^0 the reduction potential and n the number of electrons transferred in
 281 the corresponding half-reaction, F = Faraday's constant, R = gas constant, T = absolute temperature,
 282 v = voltametric scan rate (V/s), A = WE surface area (cm²), and Γ = electroactive redox protein
 283 coverage (moles/cm²). The peak currents (i_p^{ox} and i_p^{red} , **FIG. 3A**) have equal magnitude. The
 284 potentials of maximum current (E_p^{ox} and E_p^{red}) are those of E^0 . The stoichiometry of electrons
 285 transferred in the half-reaction is defined by the half-height peak width ($W_{1/2}$) using Equation (2).

$$W_{1/2} = \frac{2RT}{nF} \ln(3 + 2\sqrt{2})$$

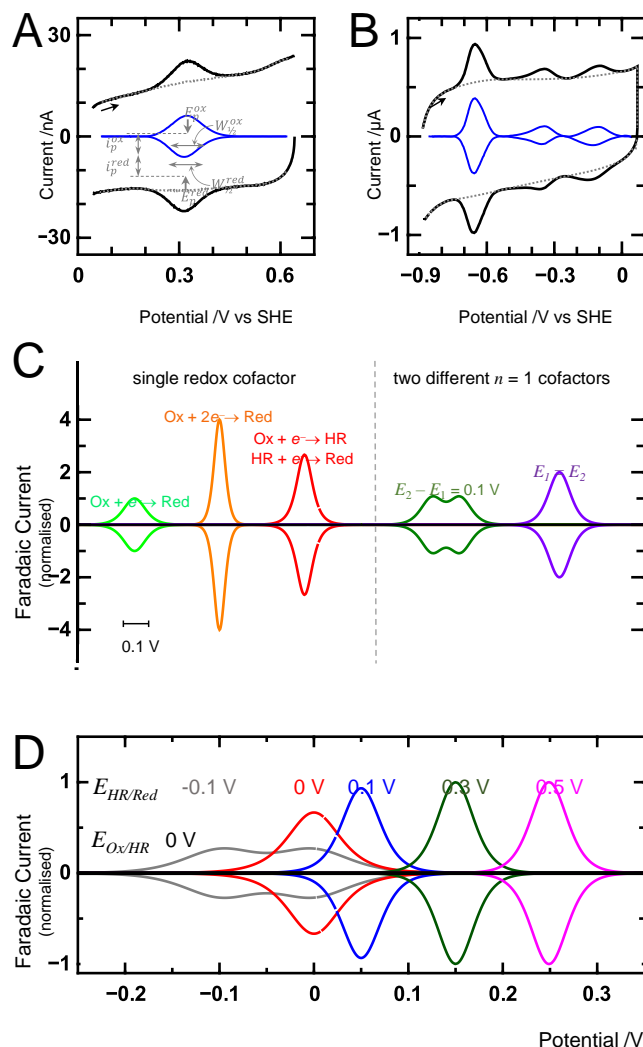


Fig. 3 | Non-catalytic peaks in the cyclic voltammetry (CV) of adsorbed proteins. **A** | Cyclic voltammogram (black) of a protein with a single $n = 1$ cofactor. Scan rate 10 mV s^{-1} , black arrow shows the scan direction. Currents due to capacitance (grey dotted line) and Faradaic currents (blue) are also shown. Peak potentials (E_p), peak currents (i_p) and half-height widths ($W_{1/2}$) are indicated for the oxidation (ox) and reduction (red) peaks. The peaks originate from a $\text{Cu}^{2+/+}$ cofactor. **B** | Cyclic voltammogram (black) of a protein with a single $n = 2$ couple and two $n = 1$ cofactors. Scan rate 19 mV s^{-1} , black arrow indicates the scan direction. Charging currents (grey dotted line) and Faradaic currents (blue) are also shown. The peaks originate from $[\text{3Fe-4S}]^{1+/0}$, $[\text{4Fe-4S}]^{2+/1+}$ and $[\text{3Fe-4S}]^{0/2-}$ cofactors in order of increasingly negative reduction potential. **C** | Examples of the Faradaic currents typically produced by protein cofactors. For a single cofactor moving between oxidised (Ox) and reduced (Red) states with $n = 1$ (light green) and $n = 2$ (orange). For a single cofactor where two sequential $n = 1$ processes convert Ox to Red via a half-reduced (HR) state (red) and the reduction potentials for the two half-reactions are equal. For two cofactors moving between their Ox and Red states in $n = 1$ processes with $E_2 - E_1 = 0.1 \text{ V}$ (dark green) and $E_1 = E_2$ (purple). **D** | Faradaic currents that can be produced by a single cofactor having two sequential $n = 1$ process where conversion of Ox to Red via a half-reduced (HR) state is described by $E_{\text{Ox/HR}} = 0 \text{ V}$ and the value for $E_{\text{HR/Red}}$ is as indicated. In practice, measured non-catalytic peaks, for example panels A and B are typically broader and less symmetrical about the potential axis than theory predicts.

288 At 25°C, $W_{1/2} = 90$ mV for $n = 1$, **FIG. 3C** green, and $W_{1/2} = 45$ mV for $n = 2$, **FIG. 3C** orange. However,
 289 pure $n = 2$ reactions are rarely observed in proteins. More often cofactors — such as flavin,
 290 molybdenum and tungsten — are described by two consecutive $n = 1$ half-reactions that link the
 291 oxidised, half-reduced and fully reduced levels. For this scenario, equations relating the peak shape
 292 and $W_{1/2}$ to the separation of reduction potentials have been presented⁵⁹. **FIG. 3D** illustrates how the
 293 form of the non-catalytic peaks is defined by the relative reduction potential values for the consecutive
 294 half-reactions in REF⁵⁹ (page 147) . In practice, small deviations from the ideal descriptions are often
 295 seen. For example, E_p^{ox} and E_p^{red} may differ slightly such that E^o is reported as the average of the
 296 measured values.

297 Because the protein film is comprised of a finite number of molecules and cofactors, the Faradaic
 298 current drops to zero when a redox reaction is complete, **FIG. 3**. The peak area defines the moles of
 299 electroactive redox cofactor ($A.\Gamma$) in the protein film through Equation (3)

Equation (3)

$$A.\Gamma = \frac{\Pi}{nFv}$$

302 where Π , the voltammetric peak area, has units of Amps.Volts (= Coulombs.Volts/sec). The areas of
 303 the oxidation and reduction peaks will be equal for a fully reversible redox process.

304 For proteins with more than one half-reaction, each reaction contributes Faradaic currents and the
 305 responses are additive^{12,48,60-64}. For the example presented in **FIG. 3B**¹², the widely spaced peaks
 306 immediately reveal three half-reactions. A cooperative $n = 2$ process appears as a prominent and
 307 narrow pair of peaks at more negative WE potentials, compared to an equivalent number of $n = 1$
 308 centres at more positive WE potentials. This distinction arises because the current magnitude varies
 309 as n^2 (Equation 1); $W_{1/2}$ varies as $90/n$ (Equation 2); and the peak area as Π (Equation 3). Multiple half-
 310 reactions are readily detected when E^o values are separated by > 0.1 V, **FIG. 3C** (dark green). When E^o
 311 values are more similar, the voltammogram may suggest a single redox centre, for example a single
 312 peak with $W_{1/2} = 90$ mV for two $n = 1$ centres with identical E^o , **FIG. 3C** (purple). In such situations fine
 313 structure within non-catalytic peaks may be indicative of multiple overlapping contributions. The
 314 ability of multiple half-reactions to describe non-catalytic peaks can be readily assessed by modelling
 315 the Faradaic currents using the equations presented above with E^o and n as variables. Such modelling
 316 can be performed in a spreadsheet programme or with iterative fitting using QSoas⁴²⁻⁴⁴. In parallel to
 317 such analysis, CV can be performed at a different pH values. E^o of one half-reaction may respond
 318 differently to pH, causing multiple, distinct non-catalytic peaks to be resolved for both oxidation and
 319 reduction.

320 The shape of non-catalytic peaks depends on the scan rate, **FIG. 4A**. For half-reactions with the form
 321 $Ox + ne^- \rightarrow Red$, the descriptions above are relevant at low scan rates, typically < 30 mV s⁻¹. At higher
 322 scan rates, the oxidation and reduction peaks become smeared across the potential axis and peak
 323 currents are smaller than predicted by extrapolating values measured at low scan rates, **FIG. 4A**. As
 324 the scan rate increases, the peak currents remain approximately equal ($i_p^{ox} \approx |i_p^{red}|$), E_p^{ox} becomes
 325 increasingly positive and E_p^{red} increasingly negative. This is because interfacial electron transfer
 326 between the protein and WE becomes -slow on voltammetric timescale. The interfacial electron
 327 transfer rate constant (k_{het}^o) can be extracted from plots of E_p^{ox} and E_p^{red} versus $\log(\text{scan rate})$ using
 328 procedures^{4,58,65} based on an exponential increase of rate with overpotential, Butler-Volmer
 329 equation¹⁵, or Marcus theory, which is more appropriate for protein cofactors with low reorganisation
 330 energy²⁰. Such plots, **FIG. 4B**, are referred to as Trumpet Plots because the deviation of E_p^{ox} and E_p^{red}

331 from E^0 has approximately equal magnitude but opposite sign⁶⁶. More complex behaviour⁶⁷ is
 332 observed for centres, such as flavins, where consecutive $n = 1$ reactions occur, sometimes separated
 333 by a protonation event.

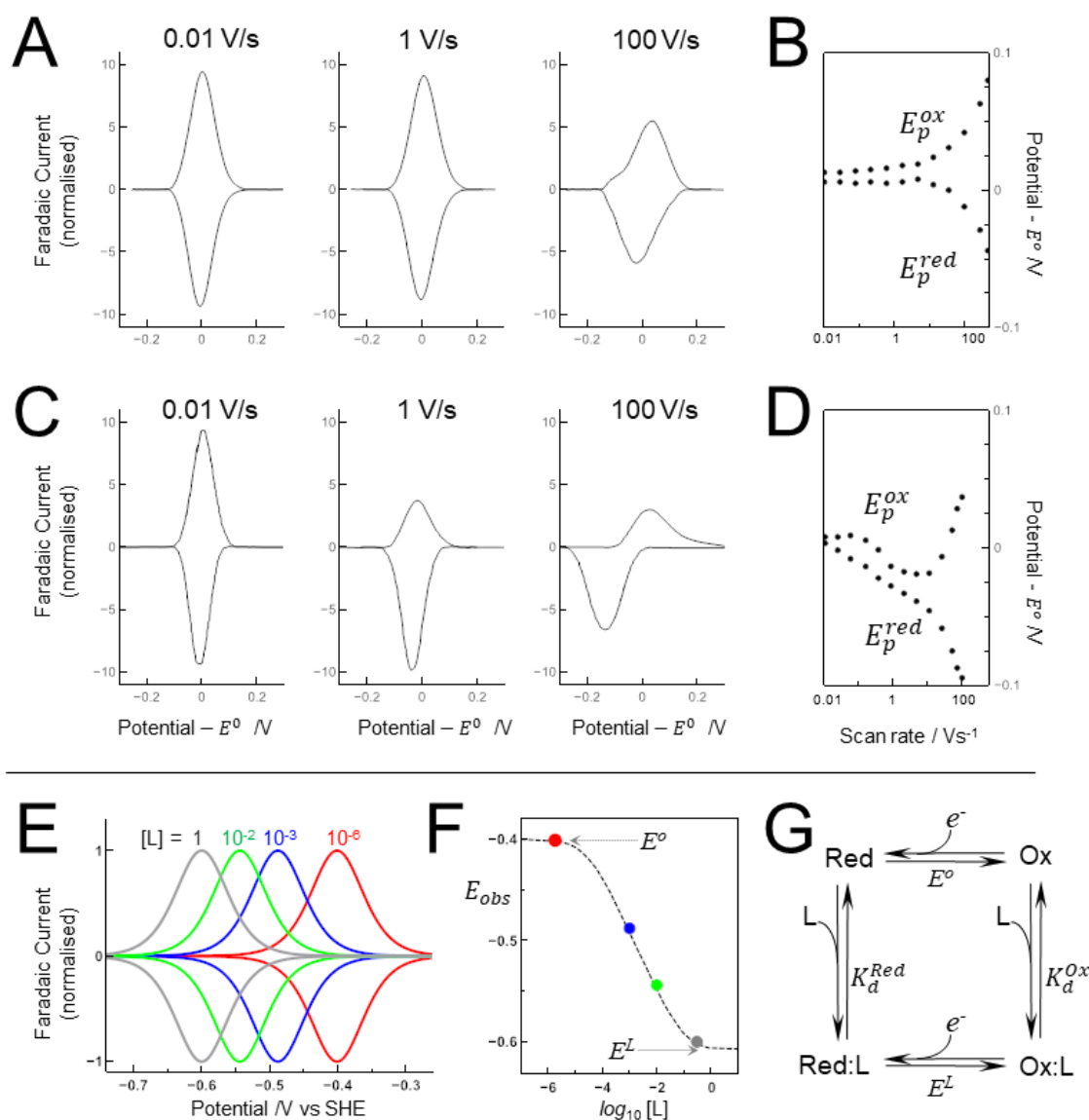


Fig. 4 | **Trumpet plots and ligand binding and unbinding.** **A** | Faradaic currents from CV at the stated scan rates illustrating behaviour typical for a reversible redox couple. **B** | Plot of peak potentials versus scan rate on a log scale for the experiment in **A**. Symmetrical displacements of E_p^{ox} and E_p^{red} about E^0 are indicative of reversible electron transfer uncomplicated by slow redox-driven chemistry. **C** | Faradaic currents from CV at the stated scan rates illustrating behaviour indicative of fast reduction followed by a slower, gated reoxidation due to ligand binding to the reduced protein. **D** | Plot of peak potentials versus scan rate on a log scale for the experiment in **C**. At higher scan rates the displacements of E_p^{ox} and E_p^{red} about E^0 are not equal. **E** | Faradaic currents from CV at the stated ligand (L) concentrations illustrating behaviour typical of ligand binding with greater affinity to an oxidised than reduced cofactor. **F** | Variation of E_{obs} for the data in **E** fit to the behaviour predicted for the dissociation constants $K_d^{Ox} = 30 \mu\text{M}$, $K_d^{Red} = 100 \text{ mM}$ and a reduction potential (E^0) of -0.4 V for a non-ligated $n = 1$ cofactor. **G** | Square-scheme illustrating ligand binding to an $n = 1$ redox centre and the corresponding thermodynamic parameters.

334

335 **Redox-driven ligand binding and unbinding**

336 CV provides several ways to identify and characterise redox-driven chemistry, such as ligand binding
337 and unbinding. One approach is to study the scan rate dependence of the non-catalytic peaks and look
338 for change in the relative magnitudes of i_p^{ox} and i_p^{red} , **FIG. 4C**⁶⁸. For this example, i_p^{ox} decreases
339 relative to $|i_p^{red}|$ at higher scan rates. The reduction peak remains well-defined. By contrast, the
340 oxidation peak is increasingly smeared towards more positive potentials. The corresponding plot of
341 E_p^{ox} and E_p^{red} versus log (scan rate) no longer resembles a trumpet, **FIG. 4D**. CV at the higher scan
342 rates reveals that reduction is fast, but re-oxidation is slower. Such behaviour is indicative of a
343 chemical change in the reduced state, which is slow to reverse, limiting the rate of re-oxidation. Using
344 the corresponding reaction scheme ($Ox + ne^- \leftrightarrow Red \leftrightarrow Red^*$), rate constants can be quantified by
345 modelling the scan rate dependence of the non-catalytic peaks^{20,22,68-71}.

346 A second way to identify ligand binding and unbinding is to study the non-catalytic peaks at low scan
347 rates in solutions of different ligand concentration (for proton binding this is different pH), **FIG. 4E**. For
348 conditions where $i_p^{ox} \approx |i_p^{red}|$ and $E_p^{ox} \approx E_p^{red}$ the observed reduction potential $E^{obs} = (E_p^{ox} + E_p^{red})/2$
349 is dependent on ligand concentration, **FIG. 4F**. To define the thermodynamic parameters describing
350 ligand binding, the data is fitted to a relevant equation^{9,68,69,72}. For example, Equation (4) describes the
351 behaviour for ligand binding to an $n = 1$ redox site:

Equation (4)

$$353 \quad E^{obs} = E^o + \frac{RT}{F} \ln \frac{\left(1 + \frac{[L]}{K_d^{Red}}\right)}{\left(1 + \frac{[L]}{K_d^{Ox}}\right)}$$

354 where E^o is the reduction potential in the absence of a ligand, $[L]$ is ligand concentration, K_d^{Ox} and
355 K_d^{Red} are dissociation constants for ligand binding to the oxidised and reduced states, respectively,
356 **FIG. 4G**. In the limit that $[L] \gg K_d^{Ox}$ and K_d^{Red} , the value of E^{obs} is equal to the reduction potential of
357 the ligand bound redox cofactor, E^L , **FIG. 4G**.

358 Redox-coupled processes can occur on timescales much longer than a single cyclic voltammogram. In
359 this situation, the chemistry and rates can be quantified by recording cyclic voltammetry continuously
360 at a constant scan rate. The appearance of peaks due to the product and disappearance of peaks due
361 to the reactant will be observed^{73,74}.

362 **Redox catalysis**

363 During PFE in the presence of a catalytic substrate, the oxidation state of an adsorbed enzyme changes
364 when the substrate is transformed to product. The WE acts as a redox partner to the enzyme, restoring
365 the initial state of the enzyme, enabling further rounds of catalysis. Electrons are no longer confined
366 to the protein film and a continuous flow of Faradaic current reports the rate of catalysis by the
367 adsorbed film. This Faradaic current is referred to as the catalytic current.

368 When formation of an oxidised product is irreversible — unidirectional catalysis — and substrate
369 binding depends on prior oxidation of the active site, the fraction of molecules that are oxidised, able
370 to bind a substrate and complete the catalytic cycle is defined by the WE potential through the Nernst
371 equation⁷⁵. The corresponding CV, **FIG. 5A**, reports a sigmoidal increase in positive catalytic current
372 when sweeping from more negative to more positive WE potentials. Similarly, CV of an adsorbed
373 enzyme performing unidirectional reductive catalysis reports a sigmoidal increase in negative catalytic

374 current on sweeping to more negative WE potentials, **FIG. 5B**. When the catalytic current-potential
 375 profiles are independent of scan direction and scan rate (typically < 20 mV s⁻¹ in PFE) steady-state
 376 catalysis is described through Equation (5)^{8,76}:

377 Equation (5)

$$378 \quad |i_{cat}(E)| = \frac{i_{lim}}{1 + \exp\left(\pm \frac{n_{cat}F}{RT}(E_{hw} - E)\right)}$$

379 Here, $i_{cat}(E)$ is the catalytic current for WE potential E ; i_{lim} is the maximum catalytic current
 380 magnitude; i_{lim}^{ox} for oxidative catalysis and i_{lim}^{red} for reductive catalysis, **FIG. 5A,B**. E_{hw} is the half-wave
 381 potential, the potential where the current is half of i_{lim} ; n_{cat} relates to the steepness of the catalytic
 382 wave and the bracketed term is positive for oxidation and negative for reduction. The values of E_{hw}
 383 and n_{cat} reveal the subtleties of redox catalysis, for example, the consequences of redox equilibration
 384 through a chain of electron transfer sites, as illustrated in **FIG. 1A**. The value of i_{lim} provides a direct
 385 measure of the maximum rate of catalysis by the protein film through the relationship $i_{lim}/F =$
 386 (Coulombs/sec) ÷ (Coulombs/mole e⁻) = mole e⁻/sec.

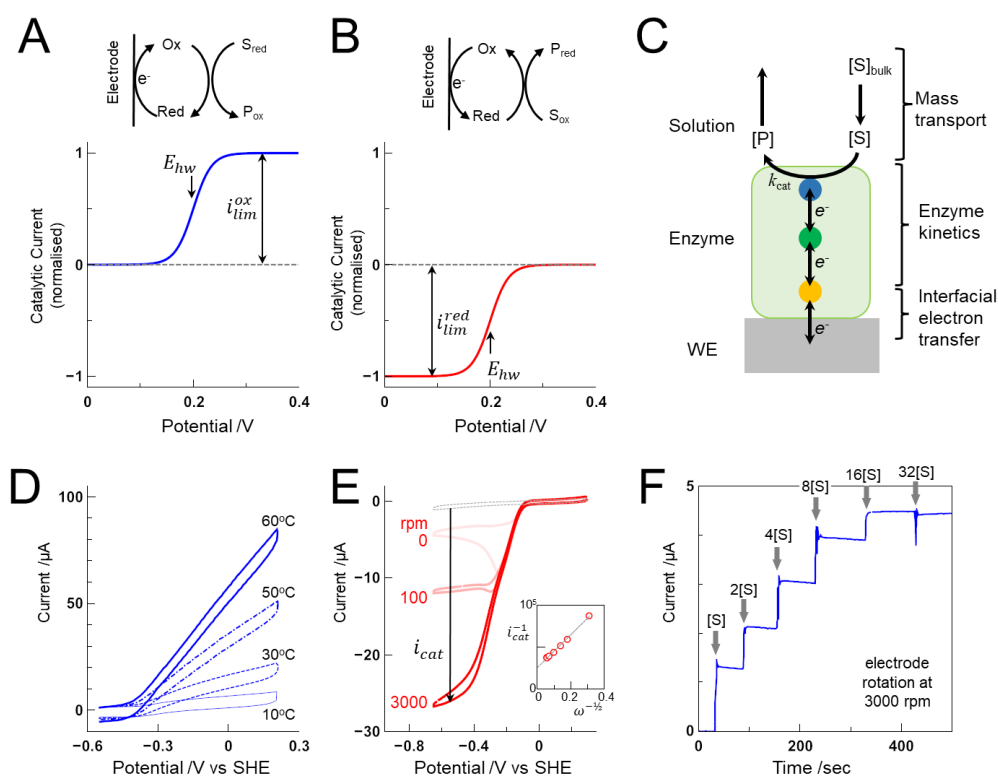


Fig. 5 | Redox catalysis. A | CV of adsorbed enzyme performing unidirectional oxidation of substrate (S) to product (P). **B** | CV of adsorbed enzyme performing unidirectional substrate reduction. **C** | Schematic illustration of processes that may determine the catalytic rate of an adsorbed enzyme: substrate transport to the electrode, enzyme kinetics (k_{cat}) and interfacial electron transfer. **D** | CV of *A. vinosum* [NiFe] hydrogenase adsorbed on a PGE electrode. Temperature as indicated for 1 atmos. H₂, pH 7. Electrode rotation rate 2500 rpm. Scan rate 1 V s⁻¹. **E** | CV of *E. coli* cytochrome *c* nitrite reductase adsorbed on a PGE electrode in 130 μM nitrite (red). Electrode rotation at the indicated rates. Scan rate 30 mV s⁻¹. CV in the absence of nitrite (grey). Arrow shows measurement of catalytic current (i_{cat}) at -550 mV for the scan towards more negative potential at 3000 rpm. Inset: Koutecky-Levich plot showing $1/i_{cat}$ measured at -550 mV against $1/(\text{angular velocity}, \omega)^{1/2}$. **F** | CA for a redox enzyme adsorbed on a PGE electrode rotated at 3000 rpm. Arrows indicate addition of substrate to the electrochemical cell to give the indicated concentration.

387 PFE of redox catalysis can provide insight into rate defining events intrinsic to the catalytic cycle of the
 388 enzyme. These events may be redox transformation of substrate in the active site, substrate binding
 389 to the enzyme, or product release from the enzyme. However, before PFE is interpreted in the context
 390 of enzyme mechanism, it is important to understand that rate defining events in catalytic PFE may also
 391 be defined by interfacial electron transfer, or delivery of substrate to the electrode via mass transport,
 392 **FIG. 5C**. Limitations due to slow electron exchange between the WE and protein can be revealed⁷⁷ by
 393 catalytic currents at high driving force, for instance at WE potentials significantly more negative or
 394 positive than the reduction potential of the substrate-product couple. For these potentials, the
 395 catalytic current magnitude has residual slope, **FIG. 5D**, instead of a plateau described by i_{lim} , **FIG.**
 396 **5A,B**. The residual slope arises due to contributions from enzymes with low rates of interfacial electron
 397 transfer compared to the enzyme turnover number, k_{cat} . As a result, the slope is greater when enzyme
 398 activity is higher. Lowering the temperature, **FIG. 5D**, or substrate concentration can reduce the
 399 limitations from slow interfacial electron transfer⁷⁷.

400 Limitations to the catalytic rate from relatively slow substrate delivery to the adsorbed enzyme are
 401 readily detected and sometimes overcome with a RDE. The RDE alleviates mass transport limitations
 402 by forced convection¹⁵. Catalytic currents that are free from mass transport limitations will be
 403 independent of the electrode rotation rate. When this cannot be achieved experimentally, catalytic
 404 currents measured at different rotation rates may be extrapolated to the catalytic current observed
 405 at infinitely high electrode rotation rate. This is typically done through a Koutecky-Levich plot with
 406 inverse catalytic current versus inverse square root of the rotation rate, presented as angular velocity,
 407 **FIG. 5E**^{78,79}. Another approach for alleviating diffusion related limitations is to reduce enzyme loading
 408 (Γ) on the electrode surface⁸⁰. This increases the diffusion layer for substrate molecules that reach the
 409 enzyme, by allowing hemispherical rather than planar diffusion⁸¹. Using an ultramicroelectrode as the
 410 WE can achieve the same outcome^{82,83}.

411 When i_{lim} is defined by the intrinsic properties of the enzyme it can be related to the substrate
 412 concentration, $[S]$, through Equation (6), the electrochemical form^{8,9,84} of the Michaelis-Menten
 413 expression¹⁷ :

414 *Equation (6)*

$$415 \quad i_{lim} = \frac{nF\Gamma k_{cat}[S]}{K_M + [S]}$$

416 where n is the number of electrons needed to convert the substrate to product; K_M is the Michaelis
 417 constant; and k_{cat} is the turnover number of the enzyme. Often, the amount of electroactive enzyme,
 418 Γ , is unknown since non-catalytic peaks cannot be discerned. However, the variation of i_{lim} with $[S]$
 419 enables quantification of K_M . This is straightforward when there is very little change of Γ during an
 420 experiment. To check changes in Γ , the enzyme coated electrode should be returned to standard
 421 conditions and i_{lim} remeasured at different time points in the experiment. When a time-dependent
 422 decay can be quantified, it is often first order^{79,85,86}. i_{lim} can be converted to values at time zero using
 423 the first order decay rate and the known time i_{lim} was measured. The time zero currents can be
 424 included in Equation (6) to quantify K_M . Such approaches are readily extended to assess changes in
 425 redox catalysis due to variations in pH and inhibitor concentration. Characteristic changes in K_M and
 426 i_{max} ($\propto k_{cat}$ for conditions where $[S] \gg K_M$) are then interpreted through standard descriptions¹⁷ of
 427 enzyme catalysis.

428 CA provides a powerful complement to CV when studying redox catalysis. Variations in i_{lim} with
429 substrate or inhibitor concentration can be defined by holding the WE at an appropriate potential and
430 performing sequential additions of the reagent to the electrochemical cell, **FIG. 5F**. During steady-
431 state catalysis, the catalytic current will be constant and independent of time following each addition.
432 When inhibitor addition leads to time-dependent changes, it suggests relatively slow inhibitor binding
433 and unbinding⁸⁷⁻⁹⁰.

434 CV can report catalytic currents for both oxidation and reduction. If the adsorbed enzyme catalyses a
435 reaction in both directions — bidirectional catalysis^{91,92} — the potential of zero current directly relates
436 to the reduction potential (E^0) of the substrate-product couple through the Nernst equation⁹²⁻⁹⁴.
437 Steady-state catalytic current profiles sometimes have additional contributions that describe a boost,
438 or attenuation, of catalysis with increasing driving force. Different explanations have been offered for
439 this behaviour⁸.

440

441 **APPLICATIONS**

442 Building on the key concepts to interpret PFE and characterise protein redox chemistry, this section
443 provides selected examples that explore these ideas in greater detail. Case studies illustrate how to
444 tailor the WE for direct electron exchange with proteins, the utility of RRDEs, and the benefits of multi-
445 disciplinary studies when interpreting complex non-typical measurements. Examples are presented
446 within a wider discussion of three research areas where PFE is making leading contributions.

447 **Biosensing**

448 In PFE, the catalytic current for an enzyme-catalysed reaction depends on the substrate concentration,
449 Equation (6). Consequently, PFE can quantify substrate concentration, which underpins the operation
450 of electrochemical biosensors⁹⁵⁻⁹⁹. Biosensors operating in this way are sometimes called third
451 generation biosensors. Earlier generations used redox mediators or co-substrates to shuttle electrons
452 between the WE and enzyme. However, small-molecule mediators can diffuse away from the WE
453 during measurements. As a result, electron exchange with the enzyme is compromised and catalytic
454 currents no longer have a simple dependence on the substrate concentration. Biosensors based on
455 direct electron transfer benefit from not requiring redox mediators or co-substrates⁹⁶. The challenge
456 of third generation biosensors is to establish stable electro-active enzyme populations that undergo
457 facile electron transfer with the WE. To address this challenge, different electrode materials and
458 surface functionalization have been explored and a variety of enzymes have been tested for their
459 ability to directly exchange electrons with these electrodes¹⁰⁰⁻¹⁰².

460 **Case Study 1**

461 Cellobiose dehydrogenase (CDH) is an enzyme that oxidises lactose, providing a basis for
462 electrochemical biosensing of a disaccharide that is prevalent in dairy products and causes symptoms
463 of lactose intolerant. CDH¹⁰³ is a monomeric enzyme, **FIG. 6A**, consisting of a catalytic dehydrogenase
464 domain (DH) with strongly a bound flavin adenine dinucleotide in the active site, and a cytochrome
465 domain (CYT) that carries a *b*-type heme. A flexible linker region connects the DH and CYT domains.
466 When CDH is adsorbed on unmodified, solid gold WEs, electrons generated by lactose oxidation in the
467 DH domain are shuttled via CYT to the WE. To improve the long-term stability and catalytic current
468 density of the biosensor, positively charged polyethyleneimine-coated gold nanoparticles (PEI-AuNPs)
469 can be deposited on the WE prior to CDH adsorption¹⁰⁴, **FIG. 6A**. The nanostructured material
470 increases the WE surface area available for enzyme adsorption. In addition, the positively charged PEI

471 binds and orientates the negatively charged CYT domain to favour direct electron exchange with the
 472 WE. CV of CDH adsorbed on PEI-AuNPs, **FIG. 6B**, reports well-defined, reversible peaks due to redox
 473 cycling of the *b*-heme in the CYT domain. Variation of the peak potentials with scan rate gives a typical
 474 trumpet plot. From this, the rate constant (k_{het}^o) for electron transfer between CYT and PEI-AuNPs can
 475 be calculated as 40 s^{-1} . The rate is higher than electron transfer between DH and CYT domains (30 s^{-1}),
 476 meaning the catalytic oxidation currents measured in the presence of lactose, **FIG. 6C**, are fully
 477 determined by the intrinsic properties of the enzyme. Catalytic currents vary linearly with lactose
 478 concentrations 1–100 μM , **FIG. 6D**. Fitting to Equation (6) gives a K_M of 0.2 mM lactose. The limit of
 479 detection is 0.33 μM lactose. CA establishes that the catalytic currents decrease by only 5.3% during
 480 ~ 300 continuous injections of lactose over 24 hours, indicating excellent long-term stability.

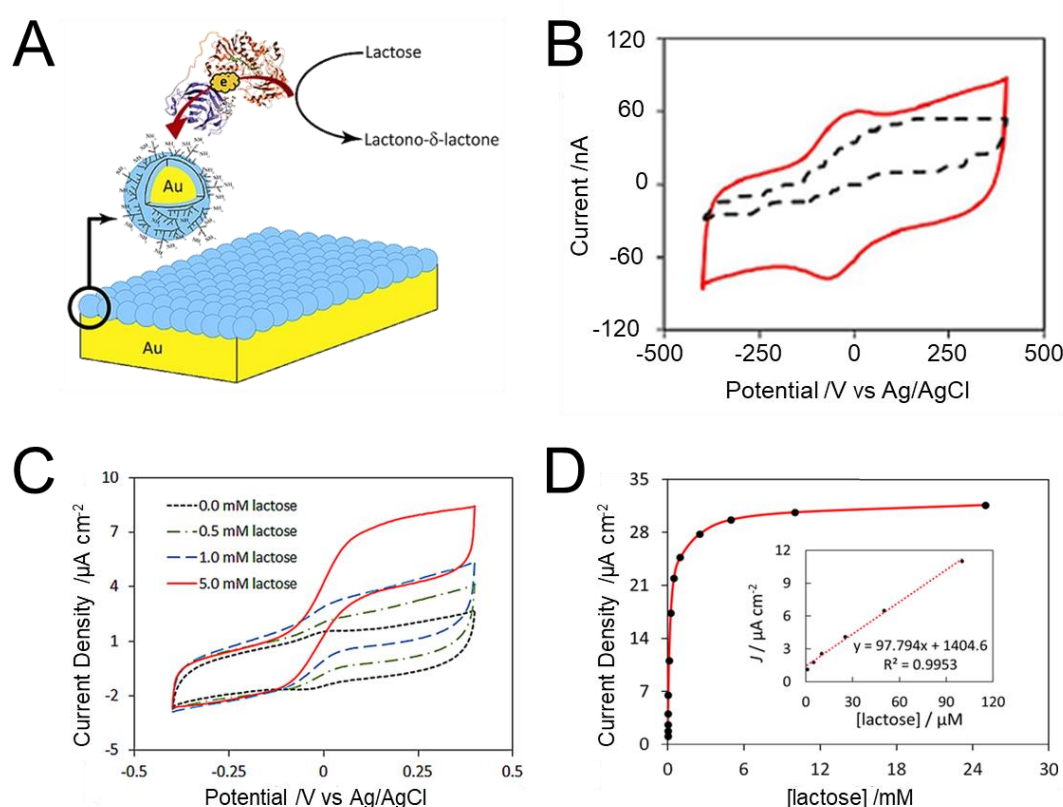


Fig. 6 | **Biosensing.** **A** | Cartoon illustrating assembly and operation of a lactose biosensor using direct electron transfer between AuNPs and the enzyme CDH. Blue: CYT domain. Red: DH domain. **B** | CV of CDH adsorbed on PEI-AuNPs on a gold WE (red line) and directly on a gold WE (black line) in 5 mM acetate, pH 4.5. Scan rate 1 mV s^{-1} . **C** | CV of PsCDH electrostatically immobilized on PEI-AuNPs on a gold WE for the indicated lactose concentrations in 5 mM acetate, pH 4.5. Scan rate 1 mV s^{-1} . **D** | Variation of catalytic response with lactose concentration as defined by CA with the WE poised at +250 mV vs. Ag/AgCl (0.1 M KCl). Inset: the response in the low-micromolar range.

481

482 Energy conversion

483 Many redox enzymes evolved to harness energy from the environment, either from sunlight during
 484 photosynthesis or chemicals during respiration. PFE replaces an enzyme's natural redox partner with
 485 a WE, creating opportunities for sustainable energy conversion. Examples include transfer of chemical
 486 to electrical energy in biofuel cells^{105,106} and the conversion of light to electricity in biophotovoltaic
 487 devices^{39,41,52,107}. For converting light to electricity, Photosystem II (PSII) attracts much interest. PSII is
 488 a membrane spanning protein complex that produces electrons, oxygen and protons simultaneously
 489 via a water-splitting photoreaction^{25,108}. PFE readily measures the light-triggered photocurrents

490 through CA by holding the biophotocathode at a desired potential and exposing it to alternating
 491 light/dark regimes. Results¹⁰⁹ comparing the WE behaviour with and without immobilized PSII are
 492 illustrated in **FIG. 7A**, where PSII was linked to a SAM coated gold WE. The SAM was terminated by
 493 nickel-nitrilotriacetic acid functionalities, enabling a direct link to PSII through a polyhistidine-tag.
 494 Another approach¹¹⁰ to immobilize PSII uses electrostatic interactions at ITO WEs, **FIG. 7B**. PSII carries
 495 a permanent dipole moment, bringing a positive charge to the region of the protein where electron
 496 exchange with the WE occurs. Consequently, ITO WEs coated with a carboxylate (negatively)
 497 terminated SAM produces higher photocurrents than equivalent WEs with no SAM or an amine
 498 (positively) terminated SAM. Photocurrents can be further enhanced and show greater stability when
 499 the carboxylate terminated SAMs incubated with PSII are exposed to covalent coupling molecules,
 500 such as carbodiimide and N-hydroxy succinimide.

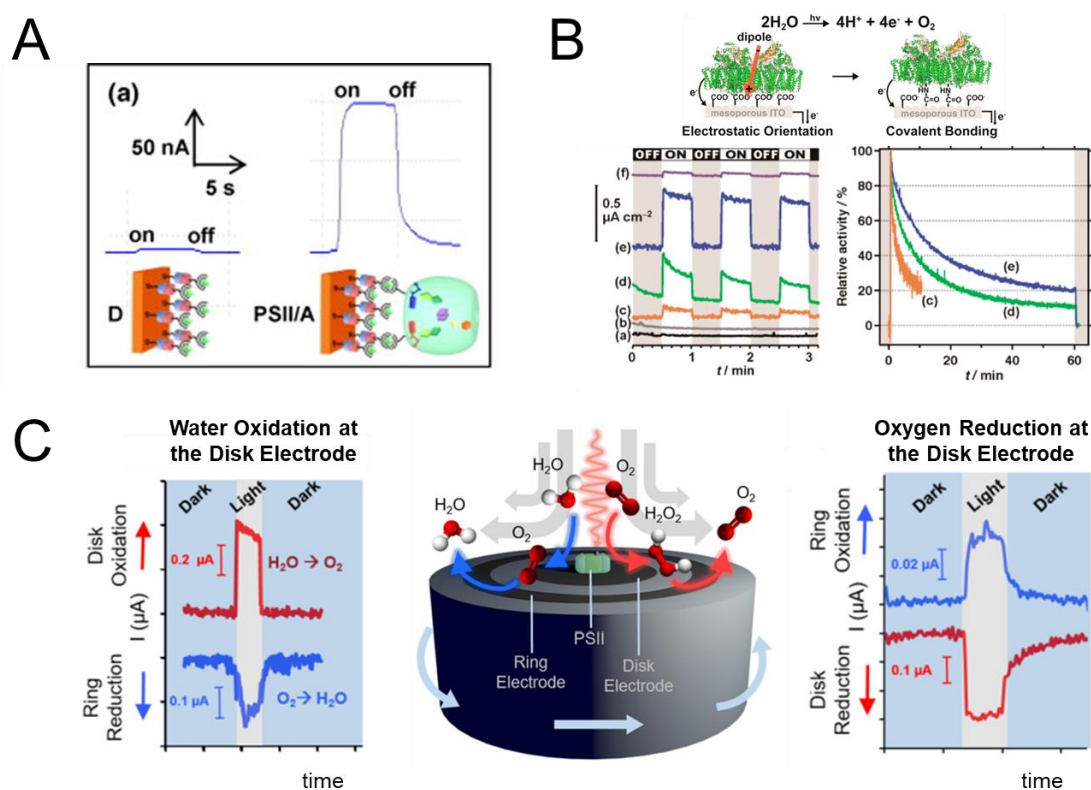


Fig. 7 | **Photoreactivity.** **A** | CA of a gold WE coated with a SAM terminated by nickel-nitrilotriacetic acid without (left) and with (right) polyhistidine tagged-PSII. WE held at 0.2 V vs. Ag/AgCl (sat. KCl). **B** | Schematic of a mesoporous ITO WE coated with a carboxylate terminated SAM onto which PSII spontaneously adsorbs (top left) and PSII covalently linked to the same electrode by carbodiimide with N-hydroxy succinimide (top right). CA (bottom left) reporting catalytic currents during cycles of irradiation by red-light for mesoporous ITO WEs coated with (a) carboxylate terminated SAM, (b) carboxylate terminated SAM treated with carbodiimide and N-hydroxy succinimide, (c) PSII (d) carboxylate terminated SAM and PSII, (e) carboxylate terminated SAM and PSII followed by exposure to the coupling agents carbodiimide with N-hydroxy succinimide. (f) is a control experiment. CA (bottom right) comparing the catalytic currents during continuous red-light irradiation for electrodes (c–e). WEs poised at +0.5 V vs NHE. **C** | Cartoon of the RRDE setup for studying PSII photochemistry (centre panel). CA revealing H_2O oxidation by PSII at the glassy carbon disk electrode (0.5 V vs SHE) and O_2 detection at the Pt ring electrode (-0.5 V vs SHE) (left panel). CA revealing reduction of O_2 by PSII at the disk electrode with H_2O_2 detected at the ring electrode. Electrode rotation at 400 rpm.

502 **Case Study 2**

503 Mechanistic insights into the photoreactivity of PSII by PFE can be achieved using a RRDE⁵⁴ and
504 potentiostat to independently control the potential applied at the disk and ring WEs. To study water
505 oxidation, PSII was adsorbed on a glassy carbon disk electrode, **FIG. 7C** (centre) and held at 0.5 V vs
506 SHE in a nitrogen-purged electrolyte solution. Positive photocurrents report light-driven oxidation by
507 PSII, **FIG. 7C** (left red). A platinum ring electrode, held at -0.5 V versus SHE, provides direct
508 quantification of oxygen liberated by PSII as a reductive current, **FIG. 7C** (left blue). Quantifying the
509 photocurrent ratios reveals that the majority (>94%) of electrons delivered to the electrode are used
510 for water oxidation by PSII. A separate experiment performed in the presence of oxygen detected
511 light-driven reduction currents from the PSII coated disk electrode, accompanied by oxidative
512 photocurrents at the ring electrode held at 0.9 V vs SHE **FIG. 7C** (right). Further experiments⁵⁴
513 established two pathways for oxygen reduction to H₂O₂ via a PSII generated superoxide (O₂⁻).

514 **Elucidating mechanisms of redox catalysis**

515 Michaelis-Menten descriptors of steady-state redox enzyme catalysis are readily defined by PFE. PFE
516 also provides a powerful route to resolve catalytic mechanisms and properties of catalytic
517 intermediates. For example, CV with substrate concentrations in large excess of K_M enables
518 examination of electron transfer within the enzyme-substrate complex when scan rates are
519 sufficiently fast to outrun the catalytic cycle¹¹¹. For studies of electron transfer within covalent enzyme
520 adducts, the presence of the covalent adduct can be confirmed by mass spectrometry immediately
521 before adsorption on the electrode and on recovery of the sample from the electrode after CV⁶⁰.

522 Arguably, the most significant contributions of PFE to understanding enzyme mechanisms are in
523 dissecting the redox driven activation and deactivation of active centres, and elucidating molecular
524 determinants of substrate access to deeply buried active centres. Such studies highlight how complex
525 behaviours observed by CV as hysteretic catalytic current-potential profiles can be resolved through
526 CA^{87,88,112,113}. An illustrative example is the behaviour of *Aquifex aeolicus* NiFe hydrogenase, which
527 catalyses H₂ oxidation⁸⁸. The CV, **FIG. 8A**, shows a peak of positive catalytic current corresponding to
528 a maximum H₂ oxidation rate. Sweeping to more positive WE potentials increases the rate of H₂
529 oxidation from the active enzyme and simultaneously drives the oxidative formation of inactive
530 enzyme. The activity of the enzyme is recovered by sweeping to more negative potentials, **Fig. 8A**,
531 meaning oxidative inactivation reverses on enzyme reduction. Activation and inactivation are slow on
532 the voltammetric timescale — an experiment at 0.3 mV/s takes about an hour — because the catalytic
533 currents are smaller when sweeping to more negative potentials than when sweeping to more positive
534 potentials. CA exposed the hydrogenase to potentials that inactivated (+65 mV) and then re-activated
535 (-60 mV) the hydrogenase such that the catalytic current decreased and then increased, **FIG. 8B**.
536 Variations in the catalytic current magnitude are directly proportional to the fraction of active enzyme.
537 Rates of activation and deactivation can be quantified by fitting to a scheme that describes the
538 reversible interconversion of active and inactive forms⁸⁸.

539 **Case Study 3**

540 PFE has contributed to multi-disciplinary studies^{89,90,114,115} of CO binding to and inhibition of
541 *Desulfovibrio fructosovorans* NiFe hydrogenase. The crystal structure of this enzyme has a
542 hydrophobic channel that allows H₂ from the surrounding solution to diffuse to the NiFe-cofactor
543 containing active site, **FIG. 8C**. The same channel allows CO to reach the active site and act as a
544 competitive inhibitor of H₂ oxidation. Insights into how the channel affects CO diffusion rates in the
545 protein were provided by CA of NiFe hydrogenase adsorbed on a rapidly rotating electrode in an

546 electrochemical cell continuously bubbled with H₂ gas⁹⁰. Introducing an aliquot of CO to the enzyme
 547 produced immediate inhibition, followed by a slow recovery of activity as CO was flushed out of the
 548 electrochemical cell, **FIG. 8D** (left). Gas binding and release rates were calculated from the
 549 corresponding amperograms.

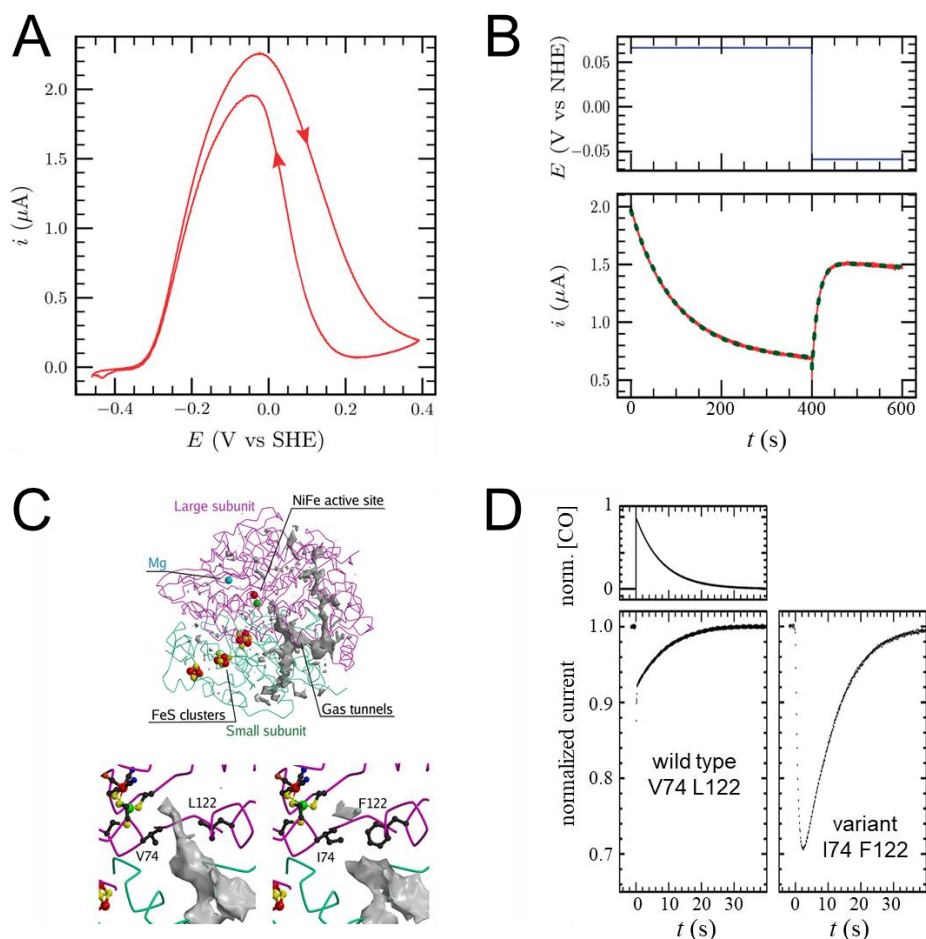


Fig. 8 | Enzyme mechanism. **A** | CV of *A. aeolicus* NiFe hydrogenase adsorbed on a graphite electrode. Electrode rotation rate 4000 rpm, scan rate 0.3 mV s⁻¹, pH 7, 40 °C, 1 atm. H₂. Arrows indicate the direction of the sweeps. **B** | CA of *A. aeolicus* NiFe hydrogenase. Electrode rotation rate 4000 rpm, pH 8, 40 °C, 1 atm. H₂. WE potential against time (upper panel). Catalytic current (red) against time and fit (green) (lower panel). Film loss during measurement accounts for the lower H₂ oxidation current at approx. 500 s that at t = 0. **C** | Structure of *D. fructosovorans* NiFe hydrogenase (upper). Detail of the gas tunnel leading to the active site in wild type enzyme (lower left) and the I74, F122 variant (lower right). **D** | CA of *D. fructosovorans* NiFe hydrogenase wild-type enzyme (left) and the L122F-V74I mutant (right) under 1 atmos. H₂ and exposed to carbon monoxide (CO) at t = 0. Enzyme adsorbed on a PGE WE. Electrode rotation rate 2000 rpm.

550 Changing residues Valine74 and Leucine122 in the gas channel to Isoleucine and Phenylalanine
 551 respectively, **FIG. 8C**, reduced the CO diffusion rate within the gas channel more than 10-fold⁹⁰, **FIG.**
 552 **8D** (right). The same mutations had minimal impact on the catalytic rate of H₂ oxidation,
 553 demonstrating that the enzyme may be engineered to resist gaseous inhibition and could be applied
 554 as an alternative to platinum catalysts in H₂ conversion technology. Furthermore, gas diffusion rates
 555 are not simply correlated with the main gas channel width defined by X-ray crystallography, **FIG. 8C**.
 556 Molecular dynamics calculations point towards CO diffusion rates being controlled at multiple
 557 locations within the gas channel¹¹⁵.

558

559 REPRODUCIBILITY AND DATA DEPOSITION

560 For a given protein, reproducibility in PFE relates to the data collected with a single film and from
561 different films. Use of data repositories has not been adopted, but published results are typically
562 available in accord with open access agreements.

563 Repeatability is related to several factors. PFE for a given protein is critically dependent on instrument
564 parameters, for example, scan rate and vertex potentials for CV, and poisoning potential and time for
565 CA. The WE rotation rate and temperature may also be defining parameters when studying redox
566 catalysis. If the protein film is prepared on a cold WE, care should be taken to ensure equilibrium
567 occurs at the desired measurement temperature before data collection. Non-reproducible values of
568 E_p and E_{hw} can arise from poorly maintained Res or gas bubbles in the electrochemical cell.

569 Unwanted and irreproducible contributions can arise from trace amounts of redox active impurities.
570 The method is sensitive, with redox signals visible for quantities $< \text{pmol}/\text{cm}^2$. All solutions should be
571 carefully defined using water and reagents of the highest possible purity. Careful cleaning of glassware
572 with, for instance, nitric acid, aqua regia, or fuming sulfuric acid is sometimes required to prevent
573 unwanted signals. Protein adsorption may be influenced by co-adsorbing impurities regardless of their
574 redox activity.

575 For a given sample and measurement condition, variations between separately prepared films include
576 differences in charging current, electroactive coverage and desorption rates. Such discrepancies can
577 be pronounced for different WE treatments. For example, extended application of a certain potential
578 to the electrode can change the electrode surface and protein behaviour. Prolonged poisoning of the WE
579 after the protein film has formed can also alter the response by changing the state of an enzyme or
580 interface. However, PFE should report the same behaviour when freshly prepared films are subject to
581 an equivalent series of chemical and measurement conditions. For example, values for E_p , $W_{1/2}$ and the
582 ratio i_p^{ox}/i_p^{red} should be consistent for CV that defines redox couples and ligand binding events. During
583 redox catalysis, critical features of the current-potential profile, such as E_{hw} and n_{cat} , should be
584 consistent. These parameters can be hard to accurately define when the population of electroactive
585 protein is low, making accurate subtraction of the charging current from the measured current
586 challenging. This challenge is amplified when the baseline deviates significantly from the theoretical
587 behaviour¹⁵ of a plate capacitor. For example, broad peaks due to oxidation or reduction of surface
588 groups are a known complication of working with graphite electrodes. The most appropriate approach
589 to baseline subtraction is still a topic of debate.

590 PFE will ideally provide the same description of redox chemistry for two or more independently
591 purified samples of a given protein. Unintended and non-reproducible signals can arise from cofactors
592 released from adsorbed or denatured proteins. This is a frequent complication in studies of
593 flavoproteins using graphite electrodes¹¹⁶. The extent of adsorption may depend on the presence or
594 identity of an affinity tag introduced to facilitate protein purification¹¹⁷.

595

596 LIMITATIONS AND OPTIMISATIONS

597 Not all redox proteins can be studied by PFE. It is essential that the protein has at least one surface
598 exposed redox centre that can act as a point of connection between the electrode and any additional
599 redox centres in the protein, **FIG. 1A**. Establishing conditions to detect and optimise PFE is like finding
600 the conditions for highly ordered protein crystallization ahead of structure resolution by X-ray

601 diffraction. The chances of success are greater with small, soluble proteins due the high percentage
602 of surface exposed redox cofactors compared to larger proteins.

603 Most electrode-protein interactions have a contribution from electrostatic interactions. The extent
604 and orientation of protein adsorption can be modulated through changes in the pH and ionic strength
605 of the protein-containing solution, the presence of a co-adsorbate, the choice of WE, and the
606 functional groups in the SAM¹¹⁸. If initial experiments have no, or small, Faradaic signals then it is
607 worth exploring different conditions to increase the electroactive population. For studies of redox
608 enzymes, the catalytic currents are proportional to the product of enzyme concentration and turnover
609 number (Equation 6). The chances of success are also increased for highly active enzymes. Because
610 catalytic currents are larger than the corresponding non-catalytic peaks, sometimes by several orders
611 of magnitude, it is always worth adding a substrate to experiments with redox enzymes to look for a
612 catalytic response. Studies of redox catalysis are informative even when there are no detectable non-
613 catalytic peaks.

614 The WE and composition of the pH buffered electrolyte solution places constraints on the explorable
615 electrochemical potential window. As the majority of PFE is performed in aqueous solution, direct
616 reduction of protons, leading to H₂ evolution at the WE, can result in large negative currents that mask
617 currents from the protein of interest. Fortunately, proton reduction is slow at most WE materials
618 specifically mentioned in this account, including gold electrodes with a well-formed SAM.
619 Consequently, the currents appear only at large overpotentials with respect to the H⁺/H₂ couple. These
620 currents tend to be smaller and appear at more negative potentials for measurements performed at
621 more alkaline pH and faster scan rates. The limiting value of positive potential is typically defined by
622 currents due to oxidation of anions from the electrolyte. It can be altered by changing the
623 concentration or identity of the ions, for instance chloride versus sulphate or chlorate. When using a
624 SAM-coated gold WE, the accessible potential window depends on the identity of the thiol and pH but
625 is typically -0.6 to +1.0 V vs SHE^{119,120}. Reductive desorption of the SAM is minimised by using scan
626 rates > 0.1 V/s.

627 Most PFE experiments aim to uncover the intrinsic properties of proteins relevant to biochemistry. To
628 ensure that the PFE does not arise from a denatured protein or dissociated cofactor, behaviour
629 reported by PFE should correlate with properties observed in complementary measurements¹²¹. For
630 redox enzymes, K_M values are readily compared to those from the classical biochemical assays.
631 Reduction potentials are typically compared to those defined by potentiometric titration of the
632 protein in solution, although small differences (< 25 mV) can be observed as the environment of an
633 adsorbed protein is not identical to that in solution. The currents measured in PFE report redox activity
634 but do not define the chemical basis of those redox events. To confidently assign a reduction potential
635 to a specific cofactor, and catalytic current to formation of a specific product, information from
636 complementary methods is needed.

637

638 **OUTLOOK**

639 PFE has seen continuous developments, with advances in electrode materials, theory, methodology
640 and in situ combination of PFE with spectroscopy and microscopy. Further improvements in these
641 areas will continue to expand the applications of PFE.

642 For some applications, PFE is limited by low electroactive coverage due to non-optimal protein
643 orientation, poor protein adsorption or because surface exposed redox co-factors are inaccessible for
644 electron exchange with planar macroscopic WEs. These challenges are sometimes overcome by

645 including conducting nanoparticles, for example carbon nanotubes, graphene oxide flakes, and gold
646 and ITO nanoparticles. Nanoparticles have two important benefits. First, they increase the surface
647 area of the WE, providing more sites for attachment and increasing protein coverage. A second benefit
648 is that nanoparticles enable more interactions with the topologically rich surface of a redox protein.
649 These versatile interactions mean nanoparticles can approach redox centres more closely than planar,
650 macroscopic electrodes.

651 As shown in Case Study 1¹⁰⁴, **FIG. 6A**, electrodes modified with nanoparticles before protein
652 application can strongly enhance the electroactive coverage. In an alternative approach, protein
653 samples can be mixed with nanoparticles and suspensions applied to the electrode. In the most
654 extreme cases, the protein-nanoparticle composite material can be considered to have become the
655 WE, with the underlying conducting material only used as a connector to the composite material. The
656 resulting higher electroactive coverage has enabled in situ spectroscopy. Examples are hydrogenase
657 studied under turn-over conditions using Fourier transform infrared spectroscopy¹²² and redox co-
658 factors characterised at various oxidation states with electron paramagnetic resonance
659 spectroscopy¹²³ or electronic absorption spectroscopy⁴⁸. Extending the use of spectroscopy in the
660 future will greatly improve the understanding of PFE and expand its applications.

661 A drawback of using nanoparticle modified WEs when studying redox catalysis — particularly if thick
662 (μm) layers are used with proteins embedded in the nanoparticle layer — is that diffusion of substrates
663 and products through nanoparticle films can be limited. Detailed descriptions of diffusion in such
664 electrodes have yet to be established. However, experimental approaches that facilitate diffusion
665 through nanoparticle layers are being developed. One example is hierarchically structured surfaces
666 with micrometre-sized pores, engineered by templating or printing techniques^{38,124}. Further
667 developments to electrode materials will improve adsorption of electroactive protein and access to
668 substrates. Electrocatalytic currents of $> 1 \text{ mA/cm}^2$ have already been obtained^{125,126}. Current densities
669 $\gg 10 \text{ mA/cm}^2$ could make PFE commercially relevant for biosynthesis of fuels and chemicals, but this
670 would require improvements in the stability of the protein films, for example by grafting^{127,128} the
671 enzyme to the electrode. New electrochemical theory and models will benefit electrode structure
672 design and further optimization¹²⁶.

673 Protein films in PFE are typically prepared for and used to study one enzyme at a time. However, many
674 interesting metabolic pathways, for example methanogenesis, contain enzyme cascades. The
675 products of PFE, such as NAD(P)H, are high-value substrates for industrially relevant enzymes and
676 biocatalytic reactions. Coupling multiple enzymes on a surface, or trapping them in small
677 compartments on the electrode, will provide new opportunities in biotechnology¹²⁹ and to control
678 points within a metabolic pathway¹³⁰⁻¹³².

679 For PFE to find widespread applications in biosensing, it is necessary to use reproducible, cheap, and
680 possibly single-use electrodes. Historically, most laboratories used home built WEs, although some
681 electrodes suitable for PFE are now commercially available. This situation is expected to stimulate
682 more research using PFE. Commercially available and affordable single-use electrodes, such as screen-
683 printed electrodes, that support reproducible PFE would benefit applications in biosensing and
684 diagnostics.

685 There are several classes of proteins that are difficult to study with PFE. The first is membrane
686 proteins, which require detergents to accommodate their amphiphilic nature and prevent
687 aggregation. However, detergent micelles in solution and around the protein can interfere with
688 protein film formation. PFE is possible for membrane proteins with large extramembranous domains
689 and relatively small transmembrane domains^{133 134}, but is increasingly difficult for complex polytopic

690 membrane proteins. Electrodes have been designed to accommodate membrane proteins within lipid
691 membranes¹³⁵, but imbedding in a lipid membrane influences the orientation of a membrane protein
692 on an electrode surface. New methods, for instance with nanoparticles¹³⁶, need to be explored to see
693 how membrane proteins can be studied with PFE.

694 A second class of oxidoreductases that are difficult to study with PFE are those that have a ping-pong
695 mechanism with active sites buried deep in the enzyme core. An example is glucose oxidase, where
696 oxygen and glucose alternatively bind to an active site flavin adenine dinucleotide (FAD) in the centre
697 of the protein. The relatively long distance between the FAD and protein surface means that direct
698 electron transfer to the WE is strongly impaired and requires special considerations, such as
699 attachment of gold nanoparticles at specific surface sites¹³⁷. There are only a few examples of PFE
700 used to study enzymes with radical intermediates, that undergo thiol-disulphide interconversion, that
701 produce radical oxygen species or that produce radical nitrogen species^{138,139}. Developing strategies
702 to interface oxidoreductases with WEs will extend the number of redox proteins and processes that
703 can be studied with PFE.

704 This manuscript has focussed on CV and CA. However, other techniques have contributed to the
705 development of PFE, notably square-wave voltammetry, differential pulse voltammetry and
706 electrochemical impedance spectroscopy^{62,140-142}. Developments in large amplitude sinusoidal
707 voltammetry or Fourier transform alternating current voltammetry have enabled differentiation of
708 various components that contribute to voltametric currents, for instance, non-Faradaic versus
709 Faradaic currents, or catalytic versus non-catalytic currents^{138,143,144}. To widen the use of these
710 techniques, they need to become available on commercial potentiostats, with freely accessible
711 software for analysis.

712

713 **Acknowledgments.**

714 JNB and LJCJ thank Professor Fraser Armstrong for inspiring and guiding their introduction to PFE,
715 and the many students and colleagues with whom they have subsequently collaborated in applying
716 and developing the technique. They are grateful for long-term funding from UK Research Councils,
717 notably BBSRC most recently through grants BB/S000704/1 and BB/S002499/1. JAJB is funded by a
718 PhD studentship from the University of East Anglia and ASC by the UKRI Biotechnology and Biological
719 Sciences Research Council Norwich Research Park Biosciences Doctoral Training Partnership [Grant
720 number BB/T008717/1].

721

722 **Competing Interests:**

723 The authors declare no competing interests

724

725 **References:**

- 726 1 Liu, J. *et al.* Metalloproteins containing cytochrome, iron-sulfur, or copper redox centers. *Chem Rev*
727 **114**, 4366-4469 (2014). <https://doi.org:10.1021/cr400479b>
- 728 2 Lippard, S. J. & Berg, J. M. *Principles of Bioinorganic Chemistry*. (University Science Books, 1994).
- 729 3 Moser, C. C., Keske, J. M., Warncke, K., Farid, R. S. & Dutton, P. L. Nature of biological electron
730 transfer. *Nature* **355**, 796-802 (1992). <https://doi.org:10.1038/355796a0>
- 731 4 Armstrong, F. A., Evans, R. M. & Megarity, C. F. Protein film electrochemistry of iron-sulfur enzymes.
732 *Meth Enzymol* **599**, 387-407 (2018). <https://doi.org:10.1016/bs.mie.2017.11.001>

- 733 5 Armstrong, F. A., Heering, H. A. & Hirst, J. Reactions of complex metalloproteins studied by protein-
734 film voltammetry. *Chem Soc Rev* **26**, 169-179 (1997). <https://doi.org:10.1039/cs9972600169>
- 735 6 Armstrong, F. A. & Wilson, G. S. Recent developments in Faradaic bioelectrochemistry. *Electrochim*
736 *Acta* **45**, 2623-2645 (2000). [https://doi.org:10.1016/S0013-4686\(00\)00342-X](https://doi.org:10.1016/S0013-4686(00)00342-X)
- 737 7 del Barrio, M. *et al.* Electrochemical investigations of hydrogenases and other enzymes that produce
738 and use solar fuels. *Acc Chem Res* **51**, 769-777 (2018). <https://doi.org:10.1021/acs.accounts.7b00622>
- 739 8 Leger, C. & Bertrand, P. Direct electrochemistry of redox enzymes as a tool for mechanistic studies.
740 *Chem Rev* **108**, 2379-2438 (2008). <https://doi.org:10.1021/cr0680742>
- 741 9 Hirst, J. Elucidating the mechanisms of coupled electron transfer and catalytic reactions by protein
742 film voltammetry. *BBA-Bioenergetics* **1757**, 225-239 (2006).
743 <https://doi.org:10.1016/j.bbabi.2006.04.002>
- 744 10 Gates, A. J. *et al.* The relationship between redox enzyme activity and electrochemical potential-
745 cellular and mechanistic implications from protein film electrochemistry. *Phys Chem Chem Phys* **13**,
746 7720-7731 (2011). <https://doi.org:10.1039/c0cp02887h>
- 747 11 Campbell-Rance, D. S., Doan, T. T. & Leopold, M. C. Sweep, step, pulse, and frequency-based
748 techniques applied to protein monolayer electrochemistry at nanoparticle interfaces. *J Electroanal*
749 *Chem* **662**, 343-354 (2011). <https://doi.org:10.1016/j.jelechem.2011.09.005>
- 750 12 Armstrong, F. A., Butt, J. N., George, S. J., Hatchikian, E. C. & Thomson, A. J. Evidence for reversible
751 multiple redox transformations of [3Fe-4S] clusters. *FEBS Lett* **259**, 15-18 (1989).
752 [https://doi.org:10.1016/0014-5793\(89\)81483-8](https://doi.org:10.1016/0014-5793(89)81483-8)
- 753 13 Feng, Z. Q., Imabayashi, S., Kakiuchi, T. & Niki, K. Electroreflectance spectroscopic study of the
754 electron-transfer rate of cytochrome c electrostatically immobilized on the omega-carboxyl
755 alkanethiol monolayer modified gold electrode. *J Electroanal Chem* **394**, 149-154 (1995).
756 [https://doi.org:10.1016/0022-0728\(95\)04058-V](https://doi.org:10.1016/0022-0728(95)04058-V)
- 757 14 Willit, J. L. & Bowden, E. F. Determination of unimolecular electron-transfer rate constants for
758 strongly adsorbed cytochrome c on tin oxide electrodes. *J Electroanal Chem* **221**, 265-274 (1987).
759 [https://doi.org:10.1016/0022-0728\(87\)80264-4](https://doi.org:10.1016/0022-0728(87)80264-4)
- 760 15 Bard, A. J. & Faulkner, L. R. *Electrochemical Methods. Fundamentals and Applications.*, (John Wiley &
761 Sons Inc., 2000).
- 762 16 Compton, R. & Banks, C. *Understanding Voltammetry* Third Edition edn, (WSPC (Europe), 2018).
- 763 17 Nelson, D. L. & Cox, M. M. *Lehninger Principles of Biochemistry.* (W. H. Freeman, 2021).
- 764 18 Colburn, A. W., Levey, K. J., O'Hare, D. & Macpherson, J. V. Lifting the lid on the potentiostat: a
765 beginner's guide to understanding electrochemical circuitry and practical operation. *Phys Chem Chem*
766 *Phys* **23**, 8100-8117 (2021). <https://doi.org:10.1039/d1cp00661d>
- 767 19 Caux, M. *et al.* PassStat, a simple but fast, precise and versatile open source potentiostat. *Hardwarex*
768 **11**, e00290 (2022). <https://doi.org:10.1016/j.ohx.2022.e00290>
- 769 20 Hirst, J. & Armstrong, F. A. Fast-scan cyclic voltammetry of protein films on pyrolytic graphite edge
770 electrodes: Characteristics of electron exchange. *Anal Chem* **70**, 5062-5071 (1998).
771 <https://doi.org:10.1021/ac980557l>
- 772 21 Jeuken, L. J. C., McEvoy, J. P. & Armstrong, F. A. Insights into gated electron-transfer kinetics at the
773 electrode-protein interface: A square wave voltammetry study of the blue copper protein azurin. *J*
774 *Phys Chem B* **106**, 2304-2313 (2002). <https://doi.org:10.1021/jp0134291>
- 775 22 Hirst, J. *et al.* Kinetics and mechanism of redox-coupled, long-range proton transfer in an iron-sulfur
776 protein. Investigation by fast-scan protein-film voltammetry. *J Am Chem Soc* **120**, 7085-7094 (1998).
777 <https://doi.org:10.1021/ja980380c>
- 778 23 Heering, H. A., Mondal, M. S. & Armstrong, F. A. Using the pulsed nature of staircase cyclic
779 voltammetry to determine interfacial electron-transfer rates of adsorbed species. *Anal Chem* **71**, 174-
780 182 (1999). <https://doi.org:10.1021/ac980844p>
- 781 24 Anantharaj, S. & Noda, S. iR drop correction in electrocatalysis: everything one needs to know! *J*
782 *Mater Chem A* **10**, 9348-9354 (2022). <https://doi.org:10.1039/d2ta01393b>
- 783 25 Kato, M., Zhang, J. Z., Paul, N. & Reisner, E. Protein film photoelectrochemistry of the water oxidation
784 enzyme photosystem II. *Chem Soc Rev* **43**, 6485-6497 (2014). <https://doi.org:10.1039/c4cs00031e>
- 785 26 Sensi, M. *et al.* Photoinhibition of FeFe hydrogenase. *ACS Catal* **7**, 7378-7387 (2017).
786 <https://doi.org:10.1021/acscatal.7b02252>
- 787 27 Murgida, D. H. In situ spectroelectrochemical investigations of electrode-confined electron-
788 transferring proteins and redox enzymes. *ACS Omega* **6**, 3435-3446 (2021).
789 <https://doi.org:10.1021/acsomega.0c05746>

- 790 28 Jeuken, L. J. C. Structure and modification of electrode materials for protein electrochemistry. *Adv*
791 *Biochem Eng Biotechnol* **158**, 43-73 (2017). https://doi.org/10.1007/10_2015_5011
- 792 29 Sahin, S. & Milton, R. D. Evolving enzymatic electrochemistry with rare or unnatural amino acids. *Curr*
793 *Opin Electrochem* **35**, 101102 (2022). <https://doi.org/10.1016/j.coelec.2022.101102>
- 794 30 Campbell, W. H., Henig, J. & Plumere, N. Affinity binding via Zinc(II) for controlled orientation and
795 electrochemistry of Histidine-tagged nitrate reductase in self-assembled monolayers. *Bioelectrochem*
796 **93**, 46-50 (2013). <https://doi.org/10.1016/j.bioelechem.2012.07.002>
- 797 31 Baffert, C. *et al.* Covalent attachment of FeFe hydrogenases to carbon electrodes for direct electron
798 transfer. *Anal Chem* **84**, 7999-8005 (2012). <https://doi.org/10.1021/ac301812s>
- 799 32 Holzinger, M., Cosnier, S. & Buzzetti, P. H. M. The versatility of pyrene and its derivatives on sp²
800 carbon nanomaterials for bioelectrochemical applications. *Synth Met* **292** (2023).
801 <https://doi.org/10.1016/j.synthmet.2022.117219>
- 802 33 Mahouche-Chergui, S., Gam-Derouich, S., Mangeney, C. & Chehimi, M. M. Aryl diazonium salts: a new
803 class of coupling agents for bonding polymers, biomacromolecules and nanoparticles to surfaces.
804 *Chem Soc Rev* **40**, 4143-4166 (2011). <https://doi.org/10.1039/c0cs00179a>
- 805 34 Love, J. C., Estroff, L. A., Kriebel, J. K., Nuzzo, R. G. & Whitesides, G. M. Self-assembled monolayers of
806 thiolates on metals as a form of nanotechnology. *Chem Rev* **105**, 1103-1169 (2005).
807 <https://doi.org/10.1021/cr0300789>
- 808 35 Yan, X. M., Tang, J., Tanner, D., Ulstrup, J. & Xiao, X. X. Direct electrochemical enzyme electron
809 transfer on electrodes modified by self-assembled molecular monolayers. *Catalysts* **10** (2020).
810 <https://doi.org/10.3390/catal10121458>
- 811 36 Doan, T. T., Freeman, M. H., Schmidt, A. R., Nguyen, N. D. T. & Leopold, M. C. Synthesis, assembly, and
812 characterization of monolayer protected gold nanoparticle films for protein monolayer
813 electrochemistry. *JoVE*, e3441 (2011). <https://doi.org/10.3791/3441>
- 814 37 Oviedo-Rouco, S. *et al.* Correlated electric field modulation of electron transfer parameters and the
815 access to alternative conformations of multifunctional cytochrome *c*. *Bioelectrochem* **143**, 107956
816 (2022). <https://doi.org/10.1016/j.bioelechem.2021.107956>
- 817 38 Mersch, D. *et al.* Wiring of Photosystem II to hydrogenase for photoelectrochemical water splitting. *J*
818 *Am Chem Soc* **137**, 8541-8549 (2015). <https://doi.org/10.1021/jacs.5b03737>
- 819 39 Morlock, S., Subramanian, S. K., Zouni, A. & Lisdat, F. Closing the green gap of photosystem I with
820 synthetic fluorophores for enhanced photocurrent generation in photobiocathodes. *Chem Sci* **14**,
821 1696-1708 (2023). <https://doi.org/10.1039/d2sc05324a>
- 822 40 Siritanaratkul, B. *et al.* Transfer of photosynthetic NADP(+)/NADPH recycling activity to a porous metal
823 oxide for highly specific, electrochemically-driven organic synthesis. *Chem Sci* **8**, 4579-4586 (2017).
824 <https://doi.org/10.1039/c7sc00850c>
- 825 41 Morlock, S., Subramanian, S. K., Zouni, A. & Lisdat, F. Bio-inorganic hybrid structures for direct
826 electron transfer to photosystem I in photobioelectrodes. *Biosens Bioelectron* **214**, 114495 (2022).
827 <https://doi.org/10.1016/j.bios.2022.114495>
- 828 42 Fourmond, V. QSoas: a versatile software for data analysis. *Anal Chem* **88**, 5050-5052 (2016).
829 <https://doi.org/10.1021/acs.analchem.6b00224>
- 830 43 Merrouch, M., Hadj-Said, J., Leger, C., Dementin, S. & Fourmond, V. Reliable estimation of the kinetic
831 parameters of redox enzymes by taking into account mass transport towards rotating electrodes in
832 protein film voltammetry experiments. *Electrochim Acta* **245**, 1059-1064 (2017).
833 <https://doi.org/10.1016/j.electacta.2017.03.114>
- 834 44 Fourmond, V. & Leger, C. Modelling the voltammetry of adsorbed enzymes and molecular catalysts.
835 *Curr Opin Electrochem* **1**, 110-120 (2017). <https://doi.org/10.1016/j.coelec.2016.11.002>
- 836 45 Heering, H. A., Wiertz, F. G. M., Dekker, C. & de Vries, S. Direct immobilization of native yeast Iso-1
837 cytochrome *c* on bare gold: Fast electron relay to redox enzymes and zeptomole protein-film
838 voltammetry. *J Am Chem Soc* **126**, 11103-11112 (2004). <https://doi.org/10.1021/ja046737w>
- 839 46 Wang, M. K., Zhao, F., Liu, Y. & Dong, S. J. Direct electrochemistry of microperoxidase at Pt
840 microelectrodes modified with carbon nanotubes. *Biosens Bioelectron* **21**, 159-166 (2005).
841 <https://doi.org/10.1016/j.bios.2004.08.012>
- 842 47 Lockwood, C. W. J. *et al.* Resolution of key roles for the distal pocket histidine in cytochrome *c* nitrite
843 reductases. *J Am Chem Soc* **137**, 3059-3068 (2015). <https://doi.org/10.1021/ja512941j>
- 844 48 Marritt, S. J. *et al.* Spectroelectrochemical characterization of a pentaheme cytochrome in solution
845 and as electrocatalytically active films on nanocrystalline metal-oxide electrodes. *J Am Chem Soc* **130**,
846 8588-8589 (2008). <https://doi.org/10.1021/ja802641a>

847 49 Reuillard, B. *et al.* High performance reduction of H₂O₂ with an electron transport decaheme
848 cytochrome on a porous ITO electrode. *J Am Chem Soc* **139**, 3324-3327 (2017).
849 <https://doi.org:10.1021/jacs.6b12437>

850 50 Ash, P. A., Hidalgo, R. & Vincent, K. A. Protein film infrared electrochemistry demonstrated for study
851 of H₂ oxidation by a [NiFe] hydrogenase. *JoVE*, e55858 (2017). <https://doi.org:10.3791/55858>

852 51 Chung, M. W. *et al.* Infrared spectroscopy coupled with protein film electrochemistry to study
853 hydrogenase inhibition by pi-acid ligands. *J Biol Inorg Chem* **19**, S879-S879 (2014).

854 52 Kornienko, N. *et al.* Advancing techniques for investigating the enzyme-electrode interface. *Acc Chem*
855 *Res* **52**, 1439-1448 (2019). <https://doi.org:10.1021/acs.accounts.9b00087>

856 53 McEvoy, J. P. & Armstrong, F. A. Protein film cryovoltammetry: demonstrations with a 7Fe ([3Fe-
857 4S]+[4Fe-4S]) ferredoxin. *Chem Commun*, 1635-1636 (1999). <https://doi.org:10.1039/a903222c>

858 54 Kornienko, N. *et al.* Oxygenic photoreactivity in Photosystem II studied by rotating ring disk
859 electrochemistry. *J Am Chem Soc* **140**, 17923-17931 (2018). <https://doi.org:10.1021/jacs.8b08784>

860 55 Fourmond, V. & Leger, C. Protein electrochemistry: questions and answers. *Adv Biochem Eng Biot*
861 **158**, 1-41 (2017). https://doi.org:10.1007/10_2015_5016

862 56 Hartshorne, R. S. *et al.* Characterization of *Shewanella oneidensis* MtrC: a cell-surface decaheme
863 cytochrome involved in respiratory electron transport to extracellular electron acceptors. *J Biol Inorg*
864 *Chem* **12**, 1083-1094 (2007). <https://doi.org:10.1007/s00775-007-0278-y>

865 57 van Wonderen, J. H., Burlat, B., Richardson, D. J., Cheesman, M. R. & Butt, J. N. The nitric oxide
866 reductase activity of cytochrome *c* nitrite reductase from *Escherichia coli*. *J Biol Chem* **283**, 9587-9594
867 (2008). <https://doi.org:10.1074/jbc.M709090200>

868 58 Laviron, E. General expression of the linear potential sweep voltammogram in the case of
869 diffusionless electrochemical systems. *J Electroanal Chem* **101**, 19-28 (1979).
870 [https://doi.org:10.1016/S0022-0728\(79\)80075-3](https://doi.org:10.1016/S0022-0728(79)80075-3)

871 59 Plichon, V. & Laviron, E. Theoretical study of a two-step reversible electrochemical reaction associated
872 with irreversible chemical reactions in thin layer linear potential sweep voltammetry. *J. Electroanal.*
873 *Chem.* **71**, 143-156 (1976). [https://doi.org:10.1016/S0022-0728\(76\)80030-7](https://doi.org:10.1016/S0022-0728(76)80030-7)

874 60 Jenner, L. P. *et al.* Reaction of thiosulfate dehydrogenase with a substrate mimic induces dissociation
875 of the cysteine heme ligand giving insights into the mechanism of oxidative catalysis. *J Am Chem Soc*
876 (2022). <https://doi.org:10.1021/jacs.2c06062>

877 61 Maiocco, S. J., Arcinas, A. J., Booker, S. J. & Elliott, S. J. Parsing redox potentials of five ferredoxins
878 found within *Thermotoga maritima*. *Protein Sci* **28**, 257-266 (2019). <https://doi.org:10.1002/pro.3547>

879 62 Zhu, W. *et al.* Structural properties and catalytic implications of the SPASM domain iron-sulfur clusters
880 in *Methylobacterium extorquens* PqqE. *J Am Chem Soc* **142**, 12620-12634 (2020).
881 <https://doi.org:10.1021/jacs.0c02044>

882 63 Rizzolo, K. *et al.* A widely distributed diheme enzyme from *Burkholderia* that displays an atypically
883 stable bis-Fe(IV) state. *Nat Commun* **10**, 1101 (2019). <https://doi.org:10.1038/s41467-019-09020-4>

884 64 Walker, L. M., Kincannon, W. M., Bandarian, V. & Elliott, S. J. Deconvoluting the reduction potentials
885 for the three [4Fe-4S] clusters in an adoMet radical SCIFF maturase. *Biochemistry* **57**, 6050-6053
886 (2018). <https://doi.org:10.1021/acs.biochem.8b00846>

887 65 Armstrong, F. A. *et al.* Fast, long-range electron-transfer reactions of a 'blue' copper protein coupled
888 non-covalently to an electrode through a stilbenyl thiolate monolayer. *Chem Commun*, 316-317
889 (2004). <https://doi.org:10.1039/b312936e>

890 66 Zitare, U. A. *et al.* The role of molecular crowding in long-range metalloprotein electron transfer:
891 Dissection into site- and scaffold-specific contributions. *Electrochim Acta* **294**, 117-125 (2019).
892 <https://doi.org:10.1016/j.electacta.2018.10.069>

893 67 Gulaboski, R., Kokoskarova, P. & Mitrev, S. Theoretical aspects of several successive two-step redox
894 mechanisms in protein-film cyclic staircase voltammetry. *Electrochim Acta* **69**, 86-96 (2012).
895 <https://doi.org:10.1016/j.electacta.2012.02.086>

896 68 Shen, B. H. *et al.* *Azotobacter vinelandii* ferredoxin I. Aspartate-15 facilitates proton transfer to the
897 reduced [3Fe-4S] cluster. *J Biol Chem* **268**, 25928-25939 (1993). [https://doi.org:10.1016/S0021-](https://doi.org:10.1016/S0021-9258(19)74476-7)
898 [9258\(19\)74476-7](https://doi.org:10.1016/S0021-9258(19)74476-7)

899 69 Butt, J. N. *et al.* Voltammetric characterization of rapid and reversible binding of an exogenous
900 thiolate ligand at a [4Fe-4S] cluster in Ferredoxin III from *Desulfovibrio africanus*. *J Am Chem Soc* **115**,
901 1413-1421 (1993). <https://doi.org:10.1021/ja00057a026>

902 70 Hirst, J., Jameson, G. N. L., Allen, J. W. A. & Armstrong, F. A. Very rapid, cooperative two-
903 electron/two-proton redox reactions of [3Fe-4S] clusters: Detection and analysis by protein-film
904 voltammetry. *J Am Chem Soc* **120**, 11994-11999 (1998). <https://doi.org:10.1021/ja981693a>
905 71 Camba, R. *et al.* Mechanisms of redox-coupled proton transfer in proteins: Role of the proximal
906 proline in reactions of the [3Fe-4S] cluster in *Azotobacter vinelandii* ferredoxin I. *Biochemistry* **42**,
907 10589-10599 (2003). <https://doi.org:10.1021/bi035021v>
908 72 Steensma, E., Heering, H. A., Hagen, W. R. & vanMierlo, C. P. M. Redox properties of wild-type,
909 Cys69Ala, and Cys69Ser *Azotobacter vinelandii* flavodoxin II as measured by cyclic voltammetry and
910 EPR spectroscopy. *Eur J Biochem* **235**, 167-172 (1996). [https://doi.org:10.1111/j.1432-](https://doi.org:10.1111/j.1432-1033.1996.00167.x)
911 [1033.1996.00167.x](https://doi.org:10.1111/j.1432-1033.1996.00167.x)
912 73 Butt, J. N., Fawcett, S. E. J., Breton, J., Thomson, A. J. & Armstrong, F. A. Electrochemical potential and
913 pH dependences of [3Fe-4S] \leftrightarrow [M3Fe-4S] cluster transformations (M = Fe, Zn, Co, and Cd) in
914 ferredoxin III from *Desulfovibrio africanus* and detection of a cluster with M = Pb. *J Am Chem Soc* **119**,
915 9729-9737 (1997). <https://doi.org:10.1021/ja971403a>
916 74 Butt, J. N., Niles, J., Armstrong, F. A., Breton, J. & Thomson, A. J. Formation and properties of a stable
917 high-potential copper-iron-sulfur cluster in a ferredoxin. *Nat Struct Biol* **1**, 427-433 (1994).
918 <https://doi.org:10.1038/nsb0794-427>
919 75 Heering, H. A., Hirst, J. & Armstrong, F. A. Interpreting the catalytic voltammetry of electroactive
920 enzymes adsorbed on electrodes. *J Phys Chem B* **102**, 6889-6902 (1998).
921 <https://doi.org:10.1021/jp981023r>
922 76 Heering, H. A., Weiner, J. H. & Armstrong, F. A. Direct detection and measurement of electron relays
923 in a multicentered enzyme: voltammetry of electrode-surface films of *E. coli* fumarate reductase, an
924 iron-sulfur flavoprotein. *J Am Chem Soc* **119**, 11628-11638 (1997). <https://doi.org:10.1021/ja9723242>
925 77 Leger, C., Jones, A. K., Albracht, S. P. J. & Armstrong, F. A. Effect of a dispersion of interfacial electron
926 transfer rates on steady state catalytic electron transport in [NiFe]-hydrogenase and other enzymes. *J*
927 *Phys Chem B* **106**, 13058-13063 (2002). <https://doi.org:10.1021/jp0265687>
928 78 Sucheta, A., Cammack, R., Weiner, J. & Armstrong, F. A. Reversible electrochemistry of fumarate
929 reductase immobilized on an electrode surface - direct voltammetric observations of redox centers
930 and their participation in rapid catalytic electron-transport. *Biochemistry* **32**, 5455-5465 (1993).
931 <https://doi.org:10.1021/bi00071a023>
932 79 Angove, H. C., Cole, J. A., Richardson, D. J. & Butt, J. N. Protein film voltammetry reveals distinctive
933 fingerprints of nitrite and hydroxylamine reduction by a cytochrome c nitrite reductase. *J Biol Chem*
934 **277**, 23374-23381 (2002). <https://doi.org:10.1074/jbc.M200495200>
935 80 Jones, A. K., Sillery, E., Albracht, S. P. J. & Armstrong, F. A. Direct comparison of the electrocatalytic
936 oxidation of hydrogen by an enzyme and a platinum catalyst. *Chem Commun*, 866-867 (2002).
937 <https://doi.org:10.1039/b201337a>
938 81 Armstrong, F. A. *et al.* Electrocatalytic reduction of hydrogen-peroxide at a stationary pyrolytic-
939 graphite electrode surface in the presence of cytochrome c peroxidase - a description based on a
940 microelectrode array model for adsorbed enzyme molecules. *Analyst* **118**, 973-978 (1993).
941 <https://doi.org:10.1039/an9931800973>
942 82 Hoeben, F. J. M. *et al.* Polymyxin-coated Au and carbon nanotube electrodes for stable [NiFe]-
943 hydrogenase film voltammetry. *Langmuir* **24**, 5925-5931 (2008). <https://doi.org:10.1021/la703984z>
944 83 Armstrong, F. A. Recent developments in dynamic electrochemical studies of adsorbed enzymes and
945 their active sites. *Curr Opin Chem Biol* **9**, 110-117 (2005). <https://doi.org:10.1016/j.cbpa.2005.02.011>
946 84 Leger, C. *et al.* Enzyme electrokinetics: Energetics of succinate oxidation by fumarate reductase and
947 succinate dehydrogenase. *Biochemistry* **40**, 11234-11245 (2001). <https://doi.org:10.1021/bi010889b>
948 85 Anderson, L. J., Richardson, D. J. & Butt, J. N. Catalytic protein film voltammetry from a respiratory
949 nitrate reductase provides evidence for complex electrochemical modulation of enzyme activity.
950 *Biochemistry* **40**, 11294-11307 (2001). <https://doi.org:10.1021/bi002706b>
951 86 Fourmond, V. *et al.* Correcting for electrocatalyst desorption and inactivation in chronoamperometry
952 experiments. *Anal Chem* **81**, 2962-2968 (2009). <https://doi.org:10.1021/ac8025702>
953 87 Gwyer, J. D., Richardson, D. J. & Butt, J. N. Resolving complexity in the interactions of redox enzymes
954 and their inhibitors: Contrasting mechanisms for the inhibition of a cytochrome c nitrite reductase
955 revealed by protein film voltammetry. *Biochemistry* **43**, 15086-15094 (2004).
956 <https://doi.org:10.1021/bi049085x>

957 88 Fourmond, V., Infossi, P., Giudici-Ortoni, M. T., Bertrand, P. & Leger, C. "Two-step"
 958 chronoamperometric method for studying the anaerobic inactivation of an oxygen tolerant NiFe
 959 hydrogenase. *J Am Chem Soc* **132**, 4848-4857 (2010). <https://doi.org/10.1021/ja910685j>
 960 89 Leger, C., Dementin, S., Bertrand, P., Rousset, M. & Guigliarelli, B. Inhibition and aerobic inactivation
 961 kinetics of *Desulfovibrio fructosovorans* NiFe hydrogenase studied by protein film voltammetry. *J Am*
 962 *Chem Soc* **126**, 12162-12172 (2004). <https://doi.org/10.1021/ja046548d>
 963 90 Leroux, F. *et al.* Experimental approaches to kinetics of gas diffusion in hydrogenase. *P Natl Acad Sci*
 964 *USA* **105**, 11188-11193 (2008). <https://doi.org/10.1073/pnas.0803689105>
 965 91 Fourmond, V., Plumere, N. & Leger, C. Reversible catalysis. *Nat Rev Chem* **5**, 348-360 (2021).
 966 <https://doi.org/10.1038/s41570-021-00268-3>
 967 92 Fourmond, V., Wiedner, E. S., Shaw, W. J. & Leger, C. Understanding and design of bidirectional and
 968 reversible catalysts of multielectron, multistep reactions. *J Am Chem Soc* **141**, 11269-11285 (2019).
 969 <https://doi.org/10.1021/jacs.9b04854>
 970 93 Armstrong, F. A. & Hirst, J. Reversibility and efficiency in electrocatalytic energy conversion and
 971 lessons from enzymes. *P Natl Acad Sci USA* **108**, 14049-14054 (2011).
 972 <https://doi.org/10.1073/pnas.1103697108>
 973 94 Kurth, J. M., Dahl, C. & Butt, J. N. Catalytic protein film electrochemistry provides a direct measure of
 974 the tetrathionate/thiosulfate reduction potential. *J Am Chem Soc* **137**, 13232-13235 (2015).
 975 <https://doi.org/10.1021/jacs.5b08291>
 976 95 Wu, Y. H. & Hu, S. S. Biosensors based on direct electron transfer in redox proteins. *Microchim Acta*
 977 **159**, 1-17 (2007). <https://doi.org/10.1007/s00604-007-0749-4>
 978 96 Das, P., Das, M., Chinnadaya, S. R., Singha, I. M. & Goswami, P. Recent advances on developing 3rd
 979 generation enzyme electrode for biosensor applications. *Biosens Bioelectron* **79**, 386-397 (2016).
 980 <https://doi.org/10.1016/j.bios.2015.12.055>
 981 97 Zuccarello, L., Barbosa, C., Todorovic, S. & Silveira, C. M. Electrocatalysis by heme enzymes-
 982 applications in biosensing. *Catalysts* **11** (2021). <https://doi.org/10.3390/catal11020218>
 983 98 Gulaboski, R., Mirceski, V., Bogeski, I. & Hoth, M. Protein film voltammetry: electrochemical
 984 enzymatic spectroscopy. A review on recent progress. *J Solid State Electrochem* **16**, 2315-2328 (2012).
 985 <https://doi.org/10.1007/s10008-011-1397-5>
 986 99 Ronkainen, N. J., Halsall, H. B. & Heineman, W. R. Electrochemical biosensors. *Chem Soc Rev* **39**, 1747-
 987 1763 (2010). <https://doi.org/10.1039/b714449k>
 988 100 Sassolas, A., Blum, L. J. & Leca-Bouvier, B. D. Immobilization strategies to develop enzymatic
 989 biosensors. *Biotechnol Adv* **30**, 489-511 (2012). <https://doi.org/10.1016/j.biotechadv.2011.09.003>
 990 101 Datta, S., Christena, L. R. & Rajaram, Y. R. S. Enzyme immobilization: an overview on techniques and
 991 support materials. *3 Biotech* **3**, 1-9 (2013). <https://doi.org/10.1007/s13205-012-0071-7>
 992 102 Bollella, P. & Katz, E. Enzyme-based biosensors: tackling electron transfer issues. *Sensors* **20** (2020).
 993 <https://doi.org/10.3390/s20123517>
 994 103 Tan, T. C. *et al.* Structural basis for cellobiose dehydrogenase action during oxidative cellulose
 995 degradation. *Nat Commun* **6** (2015). <https://doi.org/10.1038/ncomms8542>
 996 104 Tavahodi, M. *et al.* Direct electron transfer of cellobiose dehydrogenase on positively charged
 997 polyethyleneimine gold nanoparticles. *ChemPlusChem* **82**, 546-552 (2017).
 998 <https://doi.org/10.1002/cplu.201600453>
 999 105 Chen, H. *et al.* Fundamentals, applications, and future directions of bioelectrocatalysis. *Chem Rev* **120**,
 1000 12903-12993 (2020). <https://doi.org/10.1021/acs.chemrev.0c00472>
 1001 106 Xiao, X. X. *et al.* Tackling the challenges of enzymatic (bio)fuel cells. *Chem Rev* **119**, 9509-9558 (2019).
 1002 <https://doi.org/10.1021/acs.chemrev.9b00115>
 1003 107 Noll, T. & Noll, G. Strategies for "wiring" redox-active proteins to electrodes and applications in
 1004 biosensors, biofuel cells, and nanotechnology. *Chem Soc Rev* **40**, 3564-3576 (2011).
 1005 <https://doi.org/10.1039/c1cs15030h>
 1006 108 Zhang, J. Z. & Reisner, E. Advancing photosystem II photoelectrochemistry for semi-artificial
 1007 photosynthesis. *Nat Rev Chem* **4**, 6-21 (2020). <https://doi.org/10.1038/s41570-019-0149-4>
 1008 109 Terasaki, N. *et al.* Photocurrent generation properties of Histag-photosystem II immobilized on
 1009 nanostructured gold electrode. *Thin Solid Films* **516**, 2553-2557 (2008).
 1010 <https://doi.org/10.1016/j.tsf.2007.04.127>
 1011 110 Kato, M., Cardona, T., Rutherford, A. W. & Reisner, E. Covalent immobilization of oriented
 1012 Photosystem II on a nanostructured electrode for solar water oxidation. *J Am Chem Soc* **135**, 10610-
 1013 10613 (2013). <https://doi.org/10.1021/ja404699h>

1014 111 Jones, A. K., Camba, R., Reid, G. A., Chapman, S. K. & Armstrong, F. A. Interruption and time-
1015 resolution of catalysis by a flavoenzyme using fast scan protein film voltammetry. *J Am Chem Soc* **122**,
1016 6494-6495 (2000). <https://doi.org:10.1021/ja000848n>

1017 112 Orain, C. *et al.* Electrochemical measurements of the kinetics of inhibition of two FeFe Hydrogenases
1018 by O₂ demonstrate that the reaction is partly reversible. *J Am Chem Soc* **137**, 12580-12587 (2015).
1019 <https://doi.org:10.1021/jacs.5b06934>

1020 113 Field, S. J. *et al.* Reductive activation of nitrate reductases. *Dalton Trans*, 3580-3586 (2005).
1021 <https://doi.org:10.1039/b505530j>

1022 114 Liebgott, P. P. *et al.* Relating diffusion along the substrate tunnel and oxygen sensitivity in
1023 hydrogenase. *Nat Chem Biol* **6**, 63-70 (2010). <https://doi.org:10.1038/Nchembio.276>

1024 115 Wang, P. H. & Blumberger, J. Mechanistic insight into the blocking of CO diffusion in [NiFe]-
1025 hydrogenase mutants through multiscale simulation. *P Natl Acad Sci USA* **109**, 6399-6404 (2012).
1026 <https://doi.org:10.1073/pnas.1121176109>

1027 116 Heering, H. A. & Hagen, W. R. Complex electrochemistry of flavodoxin at carbon-based electrodes:
1028 Results from a combination of direct electron transfer, flavin-mediated electron transfer and
1029 comproportionation. *J Electroanal Chem* **404**, 249-260 (1996). [https://doi.org:10.1016/0022-
1030 0728\(95\)04248-2](https://doi.org:10.1016/0022-0728(95)04248-2)

1031 117 Hwang, E. T. *et al.* Exploring step-by-step assembly of nanoparticle: cytochrome biohybrid
1032 photoanodes. *ChemElectroChem* **4**, 1959-1968 (2017). <https://doi.org:10.1002/celec.201700030>

1033 118 Badiani, V. M. *et al.* Elucidating film loss and the role of hydrogen bonding of adsorbed redox enzymes
1034 by electrochemical quartz crystal microbalance analysis. *ACS Catal* **12**, 1886-1897 (2022).
1035 <https://doi.org:10.1021/acscatal.1c04317>

1036 119 Beulen, M. W. J., Kastenbergh, M. I., van Veggel, F. C. J. M. & Reinhoudt, D. N. Electrochemical stability
1037 of self-assembled monolayers on gold. *Langmuir* **14**, 7463-7467 (1998).
1038 <https://doi.org:10.1021/la981031z>

1039 120 Ramos, N. C., Medlin, J. W. & Holewinski, A. Electrochemical stability of thiolate self-assembled
1040 monolayers on Au, Pt, and Cu. *ACS Appl Mater Interfaces* **15**, 14470-14480 (2023).
1041 <https://doi.org:10.1021/acscami.3c01224>

1042 121 Milton, R. D. & Minteer, S. D. Direct enzymatic bioelectrocatalysis: differentiating between myth and
1043 reality. *J R Soc Interface* **14**, 20170253 (2017). <https://doi.org:10.1098/rsif.2017.0253>

1044 122 Ash, P. A., Kendall-Price, S. E. T. & Vincent, K. A. Unifying activity, structure, and spectroscopy of
1045 [NiFe] hydrogenases: combining techniques to clarify mechanistic understanding. *Acc Chem Res* **52**,
1046 3120-3131 (2019). <https://doi.org:10.1021/acs.accounts.9b00293>

1047 123 Abdiaziz, K., Salvadori, E., Sokol, K. P., Reisner, E. & Roessler, M. M. Protein film electrochemical EPR
1048 spectroscopy as a technique to investigate redox reactions in biomolecules. *Chem Commun* **55**, 8840-
1049 8843 (2019). <https://doi.org:10.1039/c9cc03212f>

1050 124 Chen, X. L. *et al.* 3D-printed hierarchical pillar array electrodes for high-performance semi-artificial
1051 photosynthesis. *Nat Mater* **21**, 811-818 (2022). <https://doi.org:10.1038/s41563-022-01205-5>

1052 125 Liu, Y. P. *et al.* Facile functionalization of carbon electrodes for efficient electroenzymatic hydrogen
1053 production. *JACS Au* **3**, 124-130 (2023). <https://doi.org:10.1021/jacsau.2c00551>

1054 126 Moore, E. E. *et al.* Understanding the local chemical environment of bioelectrocatalysis. *P Natl Acad
1055 Sci USA* **119**, e2114097119 (2022). <https://doi.org:10.1073/pnas.2114097119>

1056 127 Alonso-Lomillo, M. A. *et al.* Hydrogenase-coated carbon nanotubes for efficient H₂ oxidation. *Nano
1057 Lett* **7**, 1603-1608 (2007). <https://doi.org:10.1021/nl070519u>

1058 128 Rudiger, O., Abad, J. M., Hatchikian, E. C., Fernandez, V. M. & De Lacey, A. L. Oriented immobilization
1059 of *Desulfovibrio gigas* hydrogenase onto carbon electrodes by covalent bonds for nonmediated
1060 oxidation of H₂. *J Am Chem Soc* **127**, 16008-16009 (2005). <https://doi.org:10.1021/ja0554312>

1061 129 Yarman, A. *et al.* Third generation ATP sensor with enzymatic analyte recycling. *Electroanal* **26**, 2043-
1062 2048 (2014). <https://doi.org:10.1002/elan.201400231>

1063 130 Armstrong, F. A., Cheng, B. C., Herold, R. A., Megarity, C. F. & Siritanaratkul, B. From protein film
1064 electrochemistry to nanoconfined enzyme cascades and the electrochemical leaf. *Chem Rev* **123**,
1065 5421-5458 (2023). <https://doi.org:10.1021/acs.chemrev.2c00397>

1066 131 Megarity, C. F., Weald, T. R. I., Heath, R. S., Turner, N. J. & Armstrong, F. A. A nanoconfined four-
1067 enzyme cascade simultaneously driven by electrical and chemical energy, with built-in rapid, confocal
1068 recycling of NADP(H) and ATP. *ACS Catal* **12**, 8811-8821 (2022).
1069 <https://doi.org:10.1021/acscatal.2c00999>

- 1070 132 Lee, Y. S., Lim, K. & Minteer, S. D. Cascaded biocatalysis and bioelectrocatalysis: overview and recent
1071 advances. *Annu Rev Phys Chem* **72**, 467-488 (2021). [https://doi.org/10.1146/annurev-physchem-](https://doi.org/10.1146/annurev-physchem-090519-050109)
1072 [090519-050109](https://doi.org/10.1146/annurev-physchem-090519-050109)
- 1073 133 McMillan, D. G. G., Marritt, S. J., Butt, J. N. & Jeuken, L. J. C. Menaquinone-7 is specific cofactor in
1074 tetraheme quinol dehydrogenase CymA. *J Biol Chem* **287**, 14215-14225 (2012).
1075 <https://doi.org/10.1074/jbc.M112.348813>
- 1076 134 Gutierrez-Sanchez, C. *et al.* Oriented immobilization of a membrane-bound hydrogenase onto an
1077 electrode for direct electron transfer. *Langmuir* **27**, 6449-6457 (2011).
1078 <https://doi.org/10.1021/la200141t>
- 1079 135 Friedrich, M. G. *et al.* In situ monitoring of the catalytic activity of cytochrome c oxidase in a
1080 biomimetic architecture. *Biophys J* **95**, 1500-1510 (2008).
1081 <https://doi.org/10.1529/biophysj.107.122747>
- 1082 136 Meyer, T. *et al.* Evidence for distinct electron transfer processes in terminal oxidases from different
1083 origin by means of protein film voltammetry. *J Am Chem Soc* **136**, 10854-10857 (2014).
1084 <https://doi.org/10.1021/ja505126v>
- 1085 137 Holland, J. T., Lau, C., Brozik, S., Atanassov, P. & Banta, S. Engineering of glucose oxidase for direct
1086 electron transfer via site-specific gold nanoparticle conjugation. *J Am Chem Soc* **133**, 19262-19265
1087 (2011). <https://doi.org/10.1021/ja2071237>
- 1088 138 Adamson, H. *et al.* Analysis of HypD disulfide redox chemistry via optimization of Fourier Transformed
1089 ac voltammetric data. *Anal Chem* **89**, 1565-1573 (2017).
1090 <https://doi.org/10.1021/acs.analchem.6b03589>
- 1091 139 Maiocco, S. J., Grove, T. L., Booker, S. J. & Elliott, S. J. Electrochemical resolution of the [4Fe-4S]
1092 centers of the AdoMet radical enzyme BtrN: evidence of proton coupling and an unusual, low-
1093 potential auxiliary cluster. *J Am Chem Soc* **137**, 8664-8667 (2015).
1094 <https://doi.org/10.1021/jacs.5b03384>
- 1095 140 Jeuken, L. J. C., Jones, A. K., Chapman, S. K., Cecchini, G. & Armstrong, F. A. Electron-transfer
1096 mechanisms through biological redox chains in multicenter enzymes. *J Am Chem Soc* **124**, 5702-5713
1097 (2002). <https://doi.org/10.1021/ja012638w>
- 1098 141 Gulaboski, R. Theoretical contribution towards understanding specific behaviour of "simple" protein-
1099 film reactions in square-wave voltammetry. *Electroanal* **31**, 545-553 (2019).
1100 <https://doi.org/10.1002/elan.201800739>
- 1101 142 Pilz, F. H. & Kielb, P. Cyclic voltammetry, square wave voltammetry or electrochemical impedance
1102 spectroscopy? Interrogating electrochemical approaches for the determination of electron transfer
1103 rates of immobilized redox proteins *BBA Advances* **4** 100095 (2023).
1104 <https://doi.org/10.1016/j.bbadv.2023.100095>
- 1105 143 Adamson, H., Bond, A. M. & Parkin, A. Probing biological redox chemistry with large amplitude Fourier
1106 transformed ac voltammetry. *Chem Commun* **53**, 9519-9533 (2017).
1107 <https://doi.org/10.1039/c7cc03870d>
- 1108 144 Bell, C. G., Anastassiou, C. A., O'Hare, D., Parker, K. H. & Siggers, J. H. Theoretical treatment of high-
1109 frequency, large-amplitude ac voltammetry applied to ideal surface-confined redox systems.
1110 *Electrochim Acta* **64**, 71-80 (2012). <https://doi.org/10.1016/j.electacta.2011.12.088>

1111

1112

1113 **HIGHLIGHTED REFERENCES:**

1114

1115 Leger, C. & Bertrand, P. Direct electrochemistry of redox enzymes as a tool for mechanistic studies.
1116 *Chem Rev* 108, 2379-2438 (2008). <https://doi.org:10.1021/cr0680742>

1117 **This comprehensive review summarises several models developed to interpret the PFE of**
1118 **adsorbed redox proteins and enzymes, it also explains how the models are used to analyse**
1119 **experimental data.**

1120

1121 Colburn, A. W., Levey, K. J., O'Hare, D. & Macpherson, J. V. Lifting the lid on the potentiostat: a
1122 beginner's guide to understanding electrochemical circuitry and practical operation. *Phys Chem*
1123 *Chem Phys* 23, 8100-8117 (2021). <https://doi.org:10.1039/d1cp00661d>

1124 **An excellent tutorial review on the operation of potentiostats and problem-solving issues that can**
1125 **arise with electrochemical measurements.**

1126

1127 Hirst, J. & Armstrong, F. A. Fast-scan cyclic voltammetry of protein films on pyrolytic graphite edge
1128 electrodes: Characteristics of electron exchange. *Anal Chem* 70, 5062-5071 (1998).
1129 <https://doi.org:10.1021/ac980557l>

1130

1131 **Rates of interfacial electron transfer are quantified for four different proteins, the resulting**
1132 **models consider Marcus and Butler-Volmer descriptions of interfacial electron transfer and form**
1133 **the foundations for many subsequent models of more complex behaviours.**

1134

1135

1136 Baffert, C. *et al.* Covalent attachment of FeFe hydrogenases to carbon electrodes for direct electron
1137 transfer. *Anal Chem* 84, 7999-8005 (2012). <https://doi.org:10.1021/ac301812s>

1138 **An excellent introduction to the benefits and complexities of covalent attachment of enzymes to**
1139 **electrodes for PFE.**

1140

1141 Mersch, D. *et al.* Wiring of Photosystem II to hydrogenase for photoelectrochemical water splitting. *J*
1142 *Am Chem Soc* 137, 8541-8549 (2015). <https://doi.org:10.1021/jacs.5b03737>

1143 **This paper describes PFE using hierarchical inverse-opal ITO working electrodes prepared by a**
1144 **method now used by many different research groups.**

1145

1146 Kornienko, N. *et al.* Oxygenic photoreactivity in Photosystem II studied by rotating ring disk
1147 electrochemistry. *J Am Chem Soc* 140, 17923-17931 (2018). <https://doi.org:10.1021/jacs.8b08784>

1148 **An elegant example of the power of PFE to deconvolute complexity in enzyme mechanism that**
1149 **benefits from the use of a rotating ring disk electrode.**

1150

1151

1152 Laviron, E. General expression of the linear potential sweep voltammogram in the case of
1153 diffusionless electrochemical systems. *J Electroanal Chem* 101, 19-28 (1979).
1154 [https://doi.org:10.1016/S0022-0728\(79\)80075-3](https://doi.org:10.1016/S0022-0728(79)80075-3)

1155 **This landmark paper derives equations for the non-catalytic voltammetry of adsorbed redox**
1156 **centres and that are used ubiquitously in the analysis of PFE.**

1157

1158 Butt, J. N. *et al.* Voltammetric characterization of rapid and reversible binding of an exogenous
1159 thiolate ligand at a [4Fe-4S] cluster in Ferredoxin III from *Desulfovibrio africanus*. *J Am Chem Soc* 115,
1160 1413-1421 (1993). <https://doi.org:10.1021/ja00057a026>
1161 **A comprehensive illustration of how PFE can detect and quantify chemical reactions coupled to**
1162 **redox transitions (EC and CE reactions).**

1163
1164

1165 Hirst, J., Jameson, G. N. L., Allen, J. W. A. & Armstrong, F. A. Very rapid, cooperative two-
1166 electron/two-proton redox reactions of [3Fe-4S] clusters: Detection and analysis by protein-film
1167 voltammetry. *J Am Chem Soc* 120, 11994-11999 (1998). <https://doi.org:10.1021/ja981693a>
1168

1169 **An elegant account of the use of PFE to quantify the rates of redox-coupled proton (un)binding**
1170 **events.**

1171

1172 Milton, R. D. & Minteer, S. D. Direct enzymatic bioelectrocatalysis: differentiating between myth and
1173 reality. *J R Soc Interface* 14, 20170253 (2017). <https://doi.org:10.1098/rsif.2017.0253>
1174

1175 **Some important control studies that need to be done to ensure PFE responses are not due to**
1176 **artefacts such as dissociated co-factors are highlighted in the final section of this review article.**

1177
1178

1179 Ash, P. A., Kendall-Price, S. E. T. & Vincent, K. A. Unifying activity, structure, and spectroscopy of
1180 [NiFe] hydrogenases: combining techniques to clarify mechanistic understanding. *Acc Chem Res* 52,
1181 3120-3131 (2019). <https://doi.org:10.1021/acs.accounts.9b00293>
1182

1183 **An excellent review on the benefits of combining spectroscopy with PFE.**

1184
1185

1186 Chen, X. L. *et al.* 3D-printed hierarchical pillar array electrodes for high-performance semi-artificial
1187 photosynthesis. *Nat Mater* 21, 811-818 (2022). <https://doi.org:10.1038/s41563-022-01205-5>
1188

1189 **Further progress in PFE will in part depend on improved electrode materials and this paper**
1190 **describes an elegant printing technique to create (nano)structured electrodes.**

1191
1192

1193 Liu, Y. P. *et al.* Facile functionalization of carbon electrodes for efficient electroenzymatic hydrogen
1194 production. *JACS Au* 3, 124-130 (2023). <https://doi.org:10.1021/jacsau.2c00551>
1195

1196 **Application of PFE in catalysis requires high current densities and this paper describes a relatively**
1197 **easy way to achieve this with hydrogenases.**

1198

1199 **Glossary**

1200 Chronoamperometry a technique in which electric current is measured as a function of time with the
1201 WE held at a defined electric potential, or stepped between two or more defined electric potentials.

1202 Counter electrode – an electrode that carries electric current flowing in a three-electrode
1203 electrochemical cell. Electrochemical processes occurring at this electrode are not of interest.

1204 Cyclic voltammetry – a technique in which the current is measured as the WE potential is ramped
1205 linearly with time. When a defined WE potential is reached, the potential is ramped linearly in the
1206 opposite direction to return the WE to its initial potential.

1207 Faradaic current – electric current generated by the oxidation or reduction of species at a WE.

1208 Non-Faradaic current – electric current measured in an electrochemical cell that is not due to redox
1209 processes. Typically, this current arises from migration of ions in response to the electric potential
1210 applied to an electrode.

1211 Redox catalysis - the interconversion of reactants and products through a redox reaction catalysed
1212 by an enzyme. For an enzyme catalysed reaction the reactants are often referred to as substrates.

1213 Reference electrode – an electrode with a stable and defined electrode potential. The potential of
1214 the working electrode is defined relative to that of the reference electrode.

1215 Working electrode – the electrode at which redox chemistry of interest occurs in a three-electrode
1216 electrochemical cell.